An Intercomparison of Acoustic Current Meters Deployed on the Scotian Slope

A. Drozdowski and B.J.W. Greenan

Ocean and Ecosystem Sciences Division
Maritimes Region
Fisheries and Oceans Canada

Bedford Institute of Oceanography
P.O. Box 1006
Dartmouth, Nova Scotia
Canada B2Y 4A2

2012

Canadian Technical Report of Hydrography and Ocean Sciences 279

Fisheries and Oceans Canada | Pêches et Océans Canada

Canada

Canadian Technical Report of Hydrography and Ocean Sciences

Technical reports contain scientific and technical information of a type that represents a contribution to existing knowledge but which is not normally found in the primary literature. The subject matter is generally related to programs and interests of the Oceans and Science sectors of Fisheries and Oceans Canada.

Technical reports may be cited as full publications. The correct citation appears above the abstract of each report. Each report is abstracted in the data base *Aquatic Sciences and Fisheries Abstracts*.

Technical reports are produced regionally but are numbered nationally. Requests for individual reports will be filled by the issuing establishment listed on the front cover and title page.

Regional and headquarters establishments of Ocean Science and Surveys ceased publication of their various report series as of December 1981. A complete listing of these publications and the last number issued under each title are published in the *Canadian Journal of Fisheries and Aquatic Sciences*, Volume 38: Index to Publications 1981. The current series began with Report Number 1 in January 1982.

Rapport technique canadien sur l'hydrographie et les sciences océaniques

Les rapports techniques contiennent des renseignements scientifiques et techniques qui constituent une contribution aux connaissances actuelles mais que l'on ne trouve pas normalement dans les revues scientifiques. Le sujet est généralement rattaché aux programmes et intérêts des secteurs des Océans et des Sciences de Pêches et Océans Canada.

Les rapports techniques peuvent être cités comme des publications à part entière. Le titre exact figure au-dessus du résumé de chaque rapport. Les rapports techniques sont résumés dans la base de données *Résumés des sciences aquatiques et halieutiques*.

Les rapports techniques sont produits à l'échelon régional, mais numérotés à l'échelon national. Les demandes de rapports seront satisfaites par l'établissement auteur dont le nom figure sur la couverture et la page de titre.

Les établissements de l'ancien secteur des Sciences et Levés océaniques dans les régions et à l'administration centrale ont cessé de publier leurs diverses séries de rapports en décembre 1981. Vous trouverez dans l'index des publications du volume 38 du *Journal canadien des sciences halieutiques et aquatiques*, la liste de ces publications ainsi que le dernier numéro paru dans chaque catégorie. La nouvelle série a commencé avec la publication du rapport numéro 1 en janvier 1982.

Canadian Technical Report of
Hydrography and Ocean Sciences 279

2012

An Intercomparison of Acoustic Current Meters Deployed on the Scotian Slope

by

A. Drozdowski and B.J.W. Greenan

Science Branch
Maritimes Region
Fisheries and Oceans Canada

Bedford Institute of Oceanography
P. O. Box 1006
Dartmouth, Nova Scotia
Canada B2Y 4A2

© Her Majesty the Queen in Right of Canada 2012
Cat. No. Fs 97-18/279E ISSN 0711-6764

Correct Citation for this publication:
Drozdowski, A., B.J.W. Greenan. 2012. An Intercomparison of Acoustic Current Meters Deployed on the Scotian Slope. Can. Tech. Rep. Hydrogr. Ocean. Sci. 279: v + 44 pp.

TABLE OF CONTENTS

LIST OF FIGURES IV

LIST OF TABLES IV

ABSTRACT V

RÉSUMÉ V

1. INTRODUCTION 1

2. METHODS 2

A. MOORING DESIGN AND DEPLOYMENT 2

B. DATA VALIDATION 2

3. RESULTS 4

A. DATA PRESENTATION 4

B. DATA INTERCOMPARISON 5

4. CONCLUSION 7

ACKNOWLEDGMENTS 8

REFERENCES 9

TABLES 10

FIGURES 14

APPENDIX A: ADCP VERTICAL STRUCTURE AND QUALITY PARAMETERS 29

APPENDIX B: TEMPERATURE COMPARISON 38

APPENDIX C: DISTRIBUTION OF INSTRUMENT DIFFERENCES 41

APPENDIX D: LOW SPEED AMPLIFICATION OF DIRECTIONAL ERROR 43

LIST OF FIGURES

Figure 1: Location of intercomparison mooring 14
Figure 2: Schematic diagram of mooring 1697 15
Figure 3: Time series of daily averages of speed, direction and temperature. 16
Figure 4: Time series of daily averaged across and along shelf components of the current. 17
Figure 5: Progressive vector diagram for the four current meters 18
Figure 6: Normalized distribution of current meter speeds binned in 2 cm s^{-1} intervals. 19
Figure 7: Cumulative speed distribution showing the fraction of observations below particular speeds. 20
Figure 8: Cumulative speed distribution showing the exceedance probability as a function of speed. 21
Figure 9: Spectral power distribution for across and along shelf current components 22
Figure 10: Current meter scatter plot for 3 pairings of point measuring instruments 23
Figure 11: Current meter scatter plot for 3 pairings of point measuring instruments with bin 9 of the ADCP 24
Figure 12: Speed difference statistics for selected pairs. 25
Figure 13: Directional difference statistics 25
Figure 14: Across shelf current difference statistics. 26
Figure 15: Along shelf current difference statistics. 26
Figure 16: Statistics of instrument pair differences as a function of speed 27
Figure 17: Exceedance probabilities for pair absolute differences 28
Figure 18: Average echo intensity (counts) recorded by ADCP 29
Figure 19: Percent good pings recorded by ADCP 30
Figure 20: Mean and standard deviation of percent good pings for each bin 31
Figure 21: Absolute error velocity (cm s^{-1}) recorded by the ADCP. 32
Figure 22: Median and 90th percentile of absolute error velocity (cm s^{-1}) for each bin. 33
Figure 23: Vertical time structure of ADCP speed. 34
Figure 24: Vertical structure of the ADCP RMS speed. 35
Figure 25: Vertical structure of the correlation and RMS difference of each point instrument with ADCP bins. 36
Figure 26: Pressure time series from instruments 37
Figure 27: Differences between current meter and MicroCAT temperatures (1). Scotian slope deployment. 38
Figure 28: Differences between current meter and MicroCAT temperatures (2). Scotian slope deployment. 39
Figure 29: Differences between current meter. Scotian Shelf deployment 40
Figure 30: Distributions of point instrument differences. 41
Figure 31: Distributions of ADCP and point instrument differences. 42

LIST OF TABLES

Table 1: Description of current meter setup 10
Table 2: Current statistics for the period prior to ADCP battery failure 11
Table 3: Regression Statistics for point instrument pairs. 12
Table 4: Regression Statistics for point instrument-ADCP pairs 12
Table 5: Statistics of measurement differences. 13

ABSTRACT

Drozdowski, A., B.J.W. Greenan. 2012. An Intercomparison of Acoustic Current Meters Deployed on the Scotian Slope. Can. Tech. Rep. Hydrogr. Ocean. Sci. 279: v + 44 pp.

An instrumented, subsurface mooring deployed on the Scotian Slope region of the North Atlantic, provides data in low to moderate flows for a current meter intercomparison. The primary instrument being evaluated is an acoustic Doppler single-point current meter the Aanderaa Seaguard (SG) which is compared against an older-generation single-point current meter (Aanderaa RCM11) and a acoustic Doppler current profiler (ADCP). Analysis showed that the agreement in the data returned by four current meters was high. Speed and directional correlations were above 0.94 and the root mean square of speed differences was below 1.5 cm s^{-1}. Large discrepancies were uncommon with differences exceeding 5 cm s^{-1} less than 0.1% of the time. Overall, the results are similar to those reported in Drozdowski et al. (2010). Slight over-speeding of one of the Seaguards is traced to an intentional alteration in the instruments sampling strategy. There was no evidence of the RCM11 significantly under-speeding as reported by Hogg and Frye (2007).

RÉSUMÉ

Drozdowski, A., and Greenan, B.J.W. 2012. An Intercomparison of Acoustic Current Meters Deployed on the Scotian Slope. Can. Tech. Rep. Hydrogr. Ocean. Sci. 279: v + 44 p.

Un amarrage sous-marin équipé déployé dans la région du plateau néo-écossais de l'Atlantique Nord fournit des données dans un débit faible à modéré pour une comparaison corrélative des courantomètres. Le principal instrument évalué est un courantomètre à effet Doppler acoustique à point unique, l'Aanderaa Seaguard, qui est comparé à un courantomètre à point unique de génération plus ancienne (Aanderaa RCM11) et à un profileur de courant à effet Doppler. L'analyse a montré que la concordance entre les données produites par les quatre courantomètres était élevée. Les corrélations de vitesses et de directions étaient supérieures à 0,94 et la valeur efficace des différences de vitesses était inférieure à 1,5 cm s^{-1}. Les écarts importants étaient rares et les différences surpassaient 5 cm s^{-1} moins de 0,1 % du temps. Globalement, les résultats sont semblables à ceux figurant dans Drozdowski *et al.* (2010). La légère survitesse de l'un des Seaguards est attribuable à une modification intentionnelle de la stratégie d'échantillonnage des instruments. Il n'y avait aucune preuve que le RCM11 avait une sous-vitesse considérable comme l'ont signalé Hogg et Frye (2007).

1. INTRODUCTION

Accurate long time series of currents are essential for quantifying, validating and building our knowledge of the movement of water masses. It is therefore important to test the performance of the current meters deployed in the field. This is particularly true when new instruments are to replace older proven technologies. The Bedford Institute of Oceanography (BIO) has deployed a number of moorings over the decades to assess the performance of various current meters. The most recently published work was by Drozdowski et al. (2010) and the reader is referred to that report for a summary of other previous current meter intercomparison studies. The focus of the Drozdowski report (hereafter D2010) was on performance of current meters on a subsurface mooring deployed on the Scotian Shelf from 8 May to 3 June 2008, to compare two new acoustic Doppler single-point current meters: the Aanderaa Seaguard and Teledyne RDI Doppler Volume Sampler (DVS). These were compared against a mechanical current meter (Aanderaa RCM8) and an upward looking Teledyne RDI acoustic Doppler current profiler (ADCP). The intercomparison of the five current meters indicated that all instruments provide a good measure of speed and direction in a shelf environment with moderate flows, with correlation coefficients for each of speed and direction exceeding 0.96 in all cases. The root mean square (RMS) differences were in the range 1.2– 1.6 cm s^{-1} for speed, and 14-20° for direction. Vertical shear was determined to be a significant source of the differences observed over the 11 m depth interval that the current meters were deployed.

This report describes the results of a current meter inter-comparison from a 2008-2009 mooring deployment. The experiment compares simultaneous time series from current meters placed close together on the mooring line. The primary purpose of deploying this mooring was to evaluate the performance of a new single point acoustic Doppler current meter, the Aanderaa Seaguard RCM (http://www.aadi.no/Aanderaa/Products/Seaguard/default.aspx). The Seaguard employs the Aanderaa ZPulse™ technology, which transmits an acoustic pulse of several distinct frequencies to improve the data quality of the Doppler current measurements without increasing the power drain, measurement time, or pulse length (Jakobsen et al., 2008). To aid in the evaluation, older, well-established technologies which included the Aanderaa RCM11 acoustic current meter and a 307-kHz Teledyne RDI ADCP were placed near the Seagurds on the mooring line. An Aanderaa RCM8 mechanical (paddle-wheel rotor) current meter was initially planned to be deployed as well, but due to issues with the instrument before deployment it was decided to exclude it from the mooring.

This study builds on the recent results of D2010 and extends the intercomparison to the high pressure, low scatterer and moderate low flow regime of the deep Scotian slope. This study also includes a comparison of the Seaguards with the RCM11 which was not carried out in the D2010 experiment because of RCM11 instrument failure. This mooring has the added advantage of providing a much longer (nearly yearlong) time series in a much less stratified environment as compared to the D2010 deployment. As in D2010, we seek to critically assess the current speed measurements among older current meters used at the Bedford Institute of Oceanography (BIO) over the past three decades. In particular, we hope to investigate the possible 10-25% RCM11 speed underestimation reported by Hogg and Frye (2007).

The deployment site for the present study was near the Halifax Line on the Scotian Slope at the 1700 m isobaths (Figure 1). This is a site at which some previous deep moorings have been deployed by BIO. Petrie and Smith (1977) examined records from a 1967-1968 mooring program which included three records from two moorings (980 m & 1500 m depth) during the autumn of 1968. These records varied in length from 33 to 78 days and demonstrated that low-frequency flow is oriented along isobaths with some abrupt current reversals. Spectral analysis revealed peaks at the tidal and the inertial bands, and an increase in intensity towards lower frequencies. Their correlation of the two near-bottom velocity components gave a regression axis which rotated from the direction of the local isobaths by approximately 6°. Louis et al. (1982) examined current meter records from a 1976-1977 Shelf Break Experiment and observed bursts of topographic Rossby wave energy in the region of the outer continental shelf and slope north of the Gulf Stream. Deep-water kinetic energy associated with these waves appears to be uniformly distributed over the upper portion of the Scotian Rise.

This report is structured as follows. Section 2 explains the methods used in the mooring design and deployment. Section 2 also deals with data validation and data quality issues. Results and analyses are presented in Section 3, followed by conclusions in Section 4.

2. METHODS

a. Mooring Design and Deployment

The intercomparison mooring was deployed on the Scotian Shelf Slope (Figure 1) for the period of 3 Oct. 2008 – 28 Sept. 2009 in a water depth of 1700 m. Instruments were closely spaced on a taut mooring line (BIO Consecutive Mooring No. 1697, Figure 2). A detailed summary of each instrument deployed is provided in Table 1. The primary purpose of deploying this mooring was to evaluate the performance of Aanderaa Seaguard RCMs which were placed at depths of 1589m (SG33) and 1598 m (SG20). Both were set up in Spread Mode (i.e. ping continuously through the 1 h sampling interval), but two differences in set up were: 1) ping count SG33 = 100, SG20 = 300 and 2) ZPulse SG33 = Yes, SG20 = No. The other two current meters deployed on the 2009 mooring were the Aanderaa RMC11 (1595 m) and a 307-kHz Workhorse Teledyne RDI ADCP (1650m). Both of these types of instruments have been used extensively at BIO. The ADCP was set up in an upward-looking configuration and acquired 100-ping ensembles in a 1 hour spread mode. Vertical bin size was 4 m with a range of 30 bins.
All current meters provided estimates of velocity at a 1 hour sampling interval. Streamlined buoyancy packages were used along the mooring and for the ADCP mounting in order to minimize errors from mooring-related vibrations (see Hamilton et al., 1997).

b. Data Validation

A compass offset for magnetic declination (-18.27°) was applied to all instruments. The returned Seaguard's compass readings had some discrepancies. The raw data was provided to Aanderaa for processing and they returned a de-magnetized version of the data which agreed much better with the other compasses.

The four working acoustic instruments on the 2008-2009 mooring all returned reliable data as reported by the various quality control parameters of each instrument. The top Seaguard

(SG33) reported mean signal strength of -52.5 dB with a standard deviation of 1.8 dB. The bottom Seaguard (SG20) had similar values, -52.9 dB and 1.6 dB respectively. The instrument manufacturer reports a noise floor of about -71 dB which suggests a high signal-to-noise ratio (SNR) for both data sets. Previously deployed Seaguards (D2010) reported higher mean signal strength of about -36 dB which is consistent with the shallower, high scatterer environment of that deployment.

The ADCP stopped functioning on June 30th as a result of a battery failure. The presentation and analysis of all data was constrained to the period of valid ADCP data. During its operation, the ADCP reported echo intensities of between 70 and 160 counts (Appendix A, Figure 18), with highest intensity (>110) for bins below 15. Echo intensity is a measure of the signal strength intensity returned to the ADCP transducer. Percent good pings are shown in Figure 19 and Figure 20 of Appendix A. The instrument recorded percent good pings of above 95% with standard deviations of 5-10% for bins 1-15. The good pings degraded rapidly for the higher bins with bin 20 reporting 50% good pings and standard deviations of 30% Signal degradation at greater range from the transducer is expected, but is perhaps more pronounced here due to fewer scatterers in the water column at this location and depth.

The ADCP error velocity is shown in Figure 21 and Figure 22 of Appendix A. The error velocity indicates a problem with bin 1 where the median absolute value is 8 cm s^{-1}. Bin 1 is routinely rejected due to transducer ringing (pers comm. Jim Hamilton) and likewise is done here) bins 2-20 have median absolute error velocity values of <0.5-1 cm s^{-1} which is consistent with those reported by the manufacturer, see D2010). These bins do occasionally have large error velocities (max value of 30 cm s^{-1} is reported by bin 20) but the distribution is fairly tight, with 90th percentile value between 1.2 and 2.4 cm s^{-1} (Figure 22). The error velocity for bins 21-25 deteriorates with bin 25 having a median of 2 cm s^{-1} and 90th percentile of 15 cm s^{-1}. For bins above 25, the error velocity is greater than 30 cm s^{-1}.

Figure 23 in Appendix A shows the vertical time structure of the ADCP speed. The data is clearly bad in bin 1 for the entire record, and bad above bin 20 after 2000 hours, which is consistent with the data quality parameters presented above. However, bins 10-15 (at the range where current meters further up the mooring line are located) have odd band structure not seen in the quality parameters. Figure 24 shows the RMS velocity for each bin. There is decreased speed over bins 10-20. Bin 13 is particularly bad with a decrease of ~25% in the RMS velocity. Shear of this size is not expected this deep in the water column. The same anomaly can be seen in profiles of the magnitude and standard deviation of the mean velocity (not shown here). The source of contamination is not clear but side lobe reflection from the bottom of the other instruments, which would be more pronounced in the low scatterer environment here, is a possible cause. Similar loss of data quality was seen on other RAPID moorings in the area (Pers. Comm. Y. Geshelin), where only a MicroCat CTD was present ~50m above the ADCP.

Bin 9 was chosen to represent the ADCP in the comparison with the point current meters in this analysis. It is not the bin closest to the point instruments but was found to give the best correlation and RMS difference with the point instruments (see Figure 25, Appendix A). In addition this bin is just below the interval impacted by the point instruments as discussed above, and does not have the reduction in RMS speed that is seen in bins 10-19.

Figure 26 of Appendix A shows the pressure record of each instrument. The figure is plotted for illustrative purpose only. The ADCP shows a sudden 10 dbar drop in pressure about 3000 hours into the deployment. If this was the result of an entanglement or anchor displacement, one would expect to see this in all the pressure readings above. However, this is

not the case. It is interesting to note that the abrupt pressure shift coincided with loss of data quality for bins above 20. This issue is not understood but not expected have impact on the ADCP data quality or the intercomparison.

3. RESULTS

a. Data Presentation

Figure 3 shows daily averaged time series of the speed, direction and temperature data recovered from each of the current meters. The time series indicate a good overall agreement between the instruments, although SG20 consistently reports slightly higher speeds than the other instruments. Temperature comparisons are outside the main theme of this report but figures comparing recorded current meter temperatures to temperatures from the adjacent MicroCat CTD from this deployment as well as the D2010 deployment are presented in Appendix B.

Figure 4 shows the time series of velocity resolved into the along and across shelf component as determined by local bathymetry. 245° true was taken as the positive along shelf direction and the perpendicular shoreward direction was taken as positive across shelf direction. As reported by Petrie and Smith (1977), the along shelf flow has long periods of persistent flow with sudden reversals. The across shelf component fluctuates more rapidly but has little net flow.

Table 2 summarizes the current statistics for each instrument. The magnitude and direction of the mean current is 2.9-3.2 cm s^{-1} and 241-246° T. The standard deviation of the current speed ranged from 7.9 to 9.1 cm s^{-1}, which is 3 times higher than the mean. Maximum speeds recorded where around 26 cm s^{-1}. An overview of the flow is summarized with a progressive vector diagram (PVD; Figure 5). The PVD lines gradually diverge over the period of the deployment, but some of the divergence occurs in short-term events that create offsets. For example, there is a northward shift in the track of SG20 (at around -180 km on the x-axis) relative to the other instruments early in the time series and this puts it on a slightly different trajectory for the remainder of the integration.

Figure 6 shows the distribution of the measured speed, binned in 2 cm s^{-1} intervals. The majority of data (approximately 75% of the data samples) were between 2 and 12 cm s^{-1}, 5% below 2 cm s^{-1} while 20% exceeded 12 cm s^{-1}. Observations over 20 cm s^{-1} where uncommon occurring ~1% of the time (i.e. 3-4 days per year). From the distribution we see that SG20 speeds are slightly skewed towards higher speeds. A plot (Figure 7) of the low speed distribution (< 5 cm s^{-1}) from the current meters, indicates that speeds below 1 cm s^{-1} comprise about 1-2% of the measurements. RCM11 readings resolve into clearly visible bands with ~0.25 cm s^{-1} spacing. This feature is due to the limited data recording precision of this older instrument. Figure 8 focuses on the high speed distributions. Speeds over 20 cm s^{-1} are uncommon occurring 0.5% of the time for the ADCP, SG33 and RCM11 and as often as 1.5% for SG20.

Figure 9 shows the spectral power distribution resolved into the along and across shelf components. As reported by Petrie and Smith (1977), frequencies in the semidiurnal (~2 cycles per day) and inertial oscillations (~1.4 cycles per day) range dominate with the exception of the along shelf component which has a strong, low frequency (< 0.2 cycles per day) component in addition. Also the across component has a stronger semidiurnal contribution then the along component. There are no major differences in spectra between instruments, although SG20 is slightly higher for low and mid frequencies.

b. Data Intercomparison

For a more detailed analysis involving differences between instrument pairs, the instruments were divided into two groups: (1) 3 pairings of the point instruments and (2) 3 pairings of the point instruments with the ADCP bin 9 data. All the time series in the analysis were synchronized to the ADCP clock using linear interpolation to provide a total sample size of 6462 for each instrument.

Regression Analysis

Figure 10 and Figure 11 show the scatter plots and regression best-fit lines for instruments from group 1 and 2. The regression and other pair-wise statistics are summarized in Table 3 and 4. The scatter plots show high agreement between instruments. However pairs involving SG20 speeds tend slightly towards higher values for this instrument. This is best summarized in the ratio of the RMS of the speed (Table 3 and 4). SG20 is 13% higher than to RCM11, 10% higher than ADCP and 8% then SG33.

The regressions fits are excellent with the linear fit predicting most of the variance (r^2 = coefficient of determination). speed r^2 values vary from 0.94 to 0.96 (0.89 to 0.91) for group 1(2). Group 1 r^2 values are slightly higher, possibly reflecting the depth offset (and as a result different sampling volume) of bin 9 of the ADCP. Directional r^2 values are all very high (0.96-0.98) for both groups, reflecting quality measurements by all compasses. The regression fit slopes for the speed range from 0.94 to 1.02 with y-intercepts from 0.1 to 1.0 cm s^{-1}. The SG20 higher speed values are not reflected in the slope but in the y-intercept (i.e. it has a slope of 1.02 with 1 cm s^{-1} y-intercept).

Rate correlation coefficients in group 1 (2) are in the range 0.97 – 0.99 (0.94-0.95). This is very high with group 1 values slightly higher just as for the r^2 values. Directional correlations are very high for both groups (0.96-0.98), and slightly higher in the group 1 data.

Statistics and regression fits for along and across shelf components are also included in Tables 3 and 4.

Pair Point Difference Analysis

A more detailed intercomparison involves analyzing differences between specific instrument pairs. The instruments are compared by looking at statistics of velocity differences between pairs. The differences are a combined error from both instruments and therefore in general it is difficult to say for sure which instrument is producing more reliable measurements. However by subtracting out the large common part of the signal (the agreement), we focus in on the more subtle differences (the disagreement). The distributions of error differences, shown in Figure 30 and Figure 31 of Appendix C, show that the speed, along-shelf and across-shelf differences closely resemble a normal (Gaussian) distribution computed from the mean and standard deviation (STD) of the differences. The directional differences do not share this feature. This is attributable to occasional large disagreements in the compasses (as big as 100 deg.) which lead to a large STD and a broad normal distribution that is a poor fit to the data. For now, we will focus on the speed differences. The fact that the speed differences are Gaussian, implies that we can describe the distribution with just 2 numbers, the STD and the mean (or bias). The bias reflects a systematic error between differences while the STD represents a random error which could hypothetically have been reduced by increasing the ping rate or bin size or sampling

strategy (i.e. spread mode would have less variance than burst mode, and 2 instruments sampling in spread mode should have smaller STD difference). Systematic error is more difficult to correct and might reflect instrument malfunction, limitations, calibration or mooring design issues. A 3rd statistic included here is the RMS of the difference which is the combination of the mean and STD contribution (i.e. square root of the sum of squares of the mean and STD). It is interpreted as the overall agreement for the pair.

The mean, STD and RMS of the pair point differences are given in Table 5 and shown graphically in Figure 12 to Figure 15. Table 5 also contains 90^{th} and 99^{th} percentile values as well as ratios of these values with the normal distribution 90^{th} and 99^{th} percentile values. The ratios tell us how well the differences can be represented by the normal distribution (i.e. closer to 1 means more Gaussian). As expected from the distribution plots, the values for the speed differences are close to 1 (0.99 – 1.02) but not so for the directions (0.7-1.6).

The RMS speed differences for the 6 pairs is in the range of 1.0 to 1.5 cm s^{-1}, with the SG20-RCM11 and SG20-ADCPbin9 being the highest. This disagreement is small but significant at 4-6% of the peak speeds. In addition, the RMS speed difference range is consistent with the D2010 range of 1.2– 1.6 cm s^{-1}. The bias contributes significantly to the total RMS error for the 3 pairs involving SG20 where it ranges from 0.7 to1.2 cm s^{-1} (positive value indicating over-speeding for SG20). The other 3 pairs have values of under 0.5 and do not contribute significantly. The directional RMS errors are in the range 17 – 24 ° and are dominated by the STD. This range is slightly higher than in the D2010 report (13-20°). The bias as mentioned, is small (0-5 °) and consistent with D2010. The only other notable feature of the directional errors is that it is higher for group 2 (ADCP) which is consistent with what was seen with the correlation coefficient and r^2.

The bias, STD and RMS difference statistics discussed thus far are for the entire sampling period. Figure 16 shows how the statistics vary across the range of speeds. The statistics were computed over bin widths of 3 cm s^{-1} with the exception of the highest speed bin where a bin width of 9 cm s^{-1} was used to ensure sufficient sample size. Sample size in each bin ranged between a few hundred and a thousand. The bins were overlapped by 1 cm s^{-1} for the purpose of smoothing. A pair was only included in a bin if both speeds fell within the bin range. The resulting graph shows that the speed bias is flat for pairs not involving the SG20. The 3 pairs with SG20 have a linear trend of about 1 cm s^{-1} bias over the 20 cm s^{-1} speed range or 1/20. The speed STD is flat over the entire range but increases by 20% for the highest bin for group 2. The directional bias is flat over the entire speed range. However, the directional STD error has a hyperbolic profile with very high errors at low speeds (~40 °). This is consistent with D2010 and is a result of the fact that the direction is not an independent measurement but a calculation derived from the compass reading and the measurement of the velocity direction relative to the instrument frame axis. The way in which the direction in the frame axis is computed transforms the speed error into a contribution to the directional error which has a hyperbolic speed dependence (i.e. the error approaches infinity as the speed approaches zero, which makes sense since current direction is undefined when speed is zero while the compass still makes accurate readings.). The derivation to support this statement is presented in APPENDIX D. It is not an exact reproduction of the actual calculation done by the instruments but serves an illustrative purpose of how errors combine. This finding is also believed to cause the sharp deviation from the Gaussian distribution as seen previously (i.e the speed error has an amplification affect which causes extreme directional errors at low speeds). Interestingly, the RCM8 comparison in the

D2010 report had the same tendency as the acoustic instruments even though there mis-alignment of the vane was the issue at low speeds.

A final look at the pair point difference involved computing exceedance probabilities (Figure 17). This statistic is a measure of the fraction of total time that the instruments in a pair disagreed by more than a certain amount. It is immediately apparent how the SG33 – RCM11 pair agreement stands out. This pair has no speed differences over 4 cm s^{-1}, compared to speed differences of 0.2% to 1% for the other pairs. The SG20 – ADCPbin9 pair has the highest disagreement, consistent with the fact that it also had the highest RMS difference of 1.5 cm s^{-1}. Overall results are similar to those reported in the D2010 report but slightly lower probabilities (i.e. here we found < 0.1 % in excess of 5 cm s^{-1} while in D2010 it was 0.2 %). In addition, no extreme speed errors occur (i.e no errors exceed 7 cm s^{-1} while in D2010 there were a number of observations in excess of that even though the deployment was much shorter. The directional difference exceedance has occasional large values (in excess of 100°, 0.5-1 % of the time). This is slightly more than those in D2010 where differences were in excess of 100° only about 0.2% of the time. However, the overall distribution is very similar. The large directional errors are attributed to the low speed error amplification discussed above. Group 2 has slightly higher exceedance probabilities in the range 50 to 130°.

4. CONCLUSION

Results of the 2008-2009 Scotian Slope intercomparison mooring demonstrate very good performance from the 4 instruments under investigation. Speed and directional correlations were above 0.94. The RMS of the speed (direction) differences were in the range of 1.0 to 1.5 cm s^{-1} (17 to 24 °). Large speed discrepancies between instruments were uncommon with only 0.1 % of the instrument speed differences in excess of 5 cm s^{-1}. Overall, the results are similar to those reported in D2010.

There was no evidence of RCM11 significantly under-speeding as reported by Hogg and Frye (2007). Current statistics such as mean, maximum, minimum and standard deviation for this instrument are within the range of the other instruments. The best agreement was between SG33 and RCM11. RMS difference was only 0.97 cm s^{-1} for the speed and 17.8° for direction, the lowest of all the pairs. The correlation was the highest amongst the pairs at 0.98 for the speed and 0.99 for direction. The RCM11 comparison presented here is from a single deployment and includes only validations with other acoustic current meters. Hogg and Frye (2007) base their findings on extensive testing with mechanical instruments VMCM and VACM, which they consider their long standing benchmark current meters. The equivalent for us (BIO) is the RCM8. Unfortunately, we were not able to carry out a RCM8 vs. RCM11 intercomparison on the shelf mooring due to an RCM11 failure, however, two sets of earlier intercomparisons (see D2010) between these the RCM8 and RCM11 reveal high agreement (speed correlations above 0.98).

A few notable performance issues are discussed below. It was found that one of the Seaguards had a speed distribution that was slightly skewed towards higher speeds. This instrument also had the highest standard deviation of current velocity, 10% higher than the next highest, the other Seaguard from the deployment. Furthermore, the 3 instrument pairs with this Seaguard have a linear trend of about 1 cm s^{-1} in the speed difference bias over the 20 cm s^{-1}

speed range. The other pairs do not show any noticeable trend. However, the magnitude and direction of the mean flow for this instrument is consistent with the other instruments, indicating the over-speeding cancels out when long term vector averaging is used. It's suspected that the issue is related to this Seagurad having had the Zpulse sensor intentionally turned off, and is consistent with the Aanderaa finding that Zpulse reduces variance (Jakobsen et. al. 2008). An overestimation of the variance mathematically leads to larger speeds due the additional error from combining the flow velocity components. This finding also suggests that increasing the ping rate (this Seagurad was set up with a ping rate 3 times higher than the other Seaguard on this mooring) does not compensate the loss of performance from turning off the Zpulse. This is a positive finding, which suggests that using the Zpulse technology leads to better data quality and less power consumption.

The group 2 (point instruments vs ADCP) comparisons did not produce results as good as those obtained within group 1 (point instruments only). This was reflected in lower r^2, correlation coefficients and higher exceedence probabilities for large rate and direction differences. A possible explanation is that we are seeing the loss of coherence due to the vertical offset of bin 9 which was chosen as the most suitable bin for replacing the contaminated bins nearest the point instrument.

ACKNOWLEDGMENTS

Excellent support for the preparation, deployment and recovery of the moorings was provided by Technical Operations Section at the Bedford Institute of Oceanography including Rick Boyce, Murray Scotney, Adam Hartling and Jay Barthelotte. The authors would like to thank John Loder, Yuri Geshelin, Jim Hamilton and Brian Petrie for comments and guidance. We would also like to acknowledge representatives from various manufacturers who assisted with the study including Dick Butler (Aanderaa), Ivan Victoria (Aanderaa), Jerry Mullison (Teledyne RDI) and Darryl Symonds (Teledyne RDI).

REFERENCES

Drozdowski, A., B.J.W. Greenan, M.D. Scotney, J.W. Loder, and Y. Geshelin, 2010: An intercomparison of acoustic current meters deployed on the Scotian Shelf. Can. Tech. Rep. Hydrogr. Ocean. Sci. 264:vi + 53 pp.

Hamilton, J.M., G.A. Fowler and D.J. Belliveau. 1997: Mooring vibration as a source of current meter error and its correction. *J. Atmos. Oceanic. Technol.* **14**(3), 644-655.

Hogg, N. G. and D. E. Frye, 2007: Performance of a new generation of acoustic current meters. *J. Phys. Ocean.*, **37**, 148-161.

Jakobsen, T., H. Minken, and H. Furset, 2008: Improving acoustic current measurements by ZPulse technology. *Proc. of the IEEE/OES Ninth Working Conf. on Current Measurement Technology*, Charleston, SC, IEEE, 30-35.

Louis, J. P., B. D. Petrie and P. C. Smith, 1982: Observations of topographic Rossby waves on the continental margin off Nova Scotia. *J. Phys. Oceanogr.*, **12**, 47–55.

Petrie, B. D. and P. C. Smith, 1977: Low- frequency motions on the Scotian Shelf and Slope. *Atmosphere*, **15**:117-140.

TABLES

Table 1: Description of current meter setup.

Instrument	Manufacturer	Type	Depth (m)	Parameters/Sampling Strategy
Seaguard (Serial #: 33)	Aanderaa	ZPulse™ multi-frequency Doppler Current Sensor	1589	Horizontal velocity Sampling Interval: 1 hour Spread Mode Ping Count: 100 ZPulse: Yes Forward Ping: Yes Cell Size: 1.5 m
RCM11 (Serial # 595)	Aanderaa	2000 kHz narrow band Doppler current sensor	1595	Horizontal velocity Sampling Interval: 1 hour Spread Mode Ping Count: 600
Seaguard (Serial #: 20)	Aanderaa	ZPulse™ multi-frequency Doppler Current Sensor	1598	Horizontal velocity Sampling Interval: 1 hour Spread Mode Ping Count: 300 ZPulse: No Forward Ping: Yes Cell Size: 1.5 m
SBE 37 M MicroCAT (Serial # 6434)	Sea-Bird Electronics	Moored CT sensor	1600	Temperature, conductivity and depth. Sampling Interval: 10 min
Workhorse ADCP (Serial # 10942)	Teledyne RDI	300 kHz Doppler profiler	1650	Horizontal and vertical velocity # Bins: 30 Bin Size: 4 m Ensemble Interval: 1 h 1-hour Spread Mode Ping Count: 100

Table 2: Current statistics for the period prior to ADCP battery failure. All speeds in cm s^{-1}.

Statistic	SG33	RCM11	SG20	ADCPbin9
Mean Along Shelf	2.93	3.17	3.01	3.04
Mean Across Shelf	-0.21	0.05	0.08	-0.05
Mag. Mean Vel.	2.94	3.17	3.02	3.04
Dir. Mean. Vel (Deg. T)	241.0	245.9	246.5	244.1
Mean. Speed	7.81	7.4	8.53	7.63
Max. Speed	25.99	25.2	26.04	26.02
Min. Speed	0.07	0	0.12	0.1
RMS Speed	8.84	8.49	9.58	8.69
STD of (u,v)	8.34	7.87	9.09	8.14
Variance of (u,v)	69.6	61.9	82.6	66.2
Sample Size	6462	6462	6462	6462

Table 3: Regression Statistics for point instrument pairs.

SG33 vs RCM11	Slope	y-Intercept	r^2	corr.	RMS(Y)/ RMS(X)
Speed	0.971	0.634	0.956	0.978	1.041
Across	1.051	-0.261	0.955	0.977	1.076
Along	1.035	-0.354	0.973	0.986	1.026
Direction_(T)	0.978	2.194	0.980	0.990	0.990
SG20 vs RCM11	**Slope**	**y-Intercept**	**r^2**	**corr.**	**RMS(Y)/ RMS(X)**
Speed	1.020	0.986	0.946	0.973	1.129
Across	1.175	0.018	0.927	0.963	1.221
Along	1.096	-0.464	0.963	0.981	1.086
Direction_(T)	0.966	0.565	0.978	0.989	0.972
SG20 vs SG33	**Slope**	**y-Intercept**	**r^2**	**corr.**	**RMS(Y)/ RMS(X)**
Speed	1.021	0.550	0.935	0.967	1.084
Across	1.097	0.305	0.934	0.966	1.134
Along	1.045	-0.050	0.965	0.982	1.058
Direction_(T)	0.994	-2.555	0.975	0.988	0.988

Table 4: Regression Statistics for point instrument-ADCP pairs

SG33_vs_ADCPbin9	Slope	y-Intercept	r^2	Corr.	RMS(Y)/ RMS(X)
Speed	0.938	0.659	0.891	0.944	1.018
Across	0.965	-0.161	0.911	0.955	1.011
Along	1.004	-0.121	0.944	0.972	1.021
Direction_(T)	0.991	2.859	0.962	0.981	1.008
RCM11_vs_ADCPbin9	**Slope**	**y-Intercept**	**r^2**	**corr.**	**RMS(Y)/ RMS(X)**
Speed	0.955	0.114	0.910	0.954	0.977
Across	0.905	0.094	0.927	0.963	0.940
Along	0.963	0.244	0.959	0.979	0.995
Direction_(T)	1.017	0.082	0.971	0.985	1.022
SG20_vs_ADCPbin9	**Slope**	**y-Intercept**	**r^2**	**corr.**	**RMS(Y)/ RMS(X)**
Speed	1.000	0.899	0.908	0.953	1.103
Across	1.097	0.130	0.915	0.956	1.147
Along	1.074	-0.252	0.955	0.977	1.080
Direction_(T)	0.979	1.020	0.968	0.984	0.988

Table 5: Statistics of measurement differences. All speeds in cm s^{-1} and directions in degrees. The last 4 columns are the 90th and 99th percentile value as well as ratios of these values with the normal distribution 90th and 99th percentile values.

SG33	-	**RCM11**					
	mean	*STD*	*RMS*	*p-90*	*p-99*	*p-90 norm*	*p-99 norm*
R-Speed	0.416	0.880	0.973	1.588	2.514	0.993	0.998
Direction	-1.665	17.839	17.915	21.613	70.152	0.732	1.562
Across	-0.258	1.094	1.124	1.854	2.851	0.998	0.958
Along	-0.242	1.118	1.143	1.868	3.079	0.987	1.007
SG20	-	**RCM11**					
R-Speed	1.130	1.019	1.522	2.427	3.499	1.006	1.010
Direction	-5.350	18.949	19.688	25.008	73.187	0.731	1.474
Across	0.027	1.753	1.753	2.856	4.570	0.997	1.020
Along	-0.159	1.496	1.505	2.450	4.100	0.991	1.046
SG20	-	**SG33**					
R-Speed	0.714	1.115	1.324	2.164	3.371	0.998	1.011
Direction	-3.685	19.408	19.754	25.030	77.090	0.753	1.486
Across	0.285	1.551	1.577	2.581	4.174	0.996	1.028
Along	0.083	1.357	1.359	2.203	3.696	0.984	1.055
SG33	-	**ADCPbin9**					
R-Speed	0.187	1.392	1.404	2.301	3.628	0.990	0.993
Direction	1.288	24.735	24.767	33.000	109.289	0.808	1.693
Across	-0.159	1.511	1.519	2.465	4.106	0.994	1.026
Along	-0.110	1.567	1.571	2.570	4.238	1.000	1.030
RCM11	-	**ADCPbin9**					
R-Speed	-0.229	1.263	1.284	2.101	3.386	1.000	1.018
Direction	3.064	21.988	22.199	27.712	98.056	0.750	1.695
Across	0.099	1.352	1.355	2.206	3.564	0.989	1.010
Along	0.132	1.309	1.316	2.156	3.386	1.002	0.996
SG20	-	**ADCPbin9**					
R-Speed	0.901	1.322	1.599	2.596	4.025	1.016	1.015
Direction	-2.676	22.366	22.524	29.138	95.315	0.772	1.637
Across	0.126	1.741	1.745	2.888	4.590	1.011	1.015
Along	-0.027	1.577	1.577	2.566	4.071	0.988	0.993

FIGURES

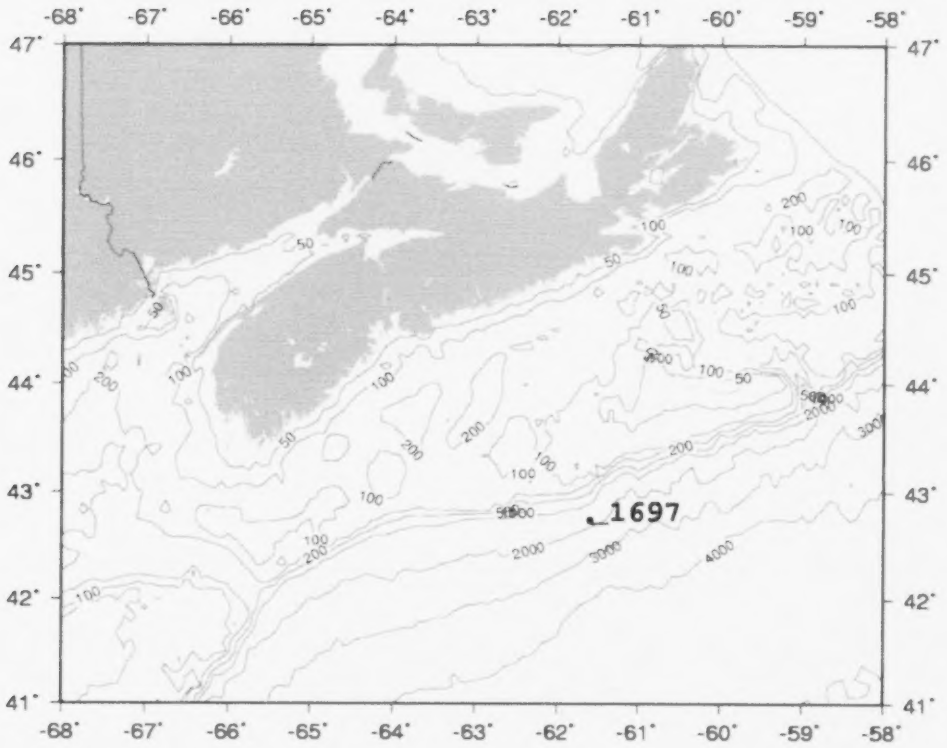

Figure 1: Location of intercomparison mooring. Depth contours in meters.

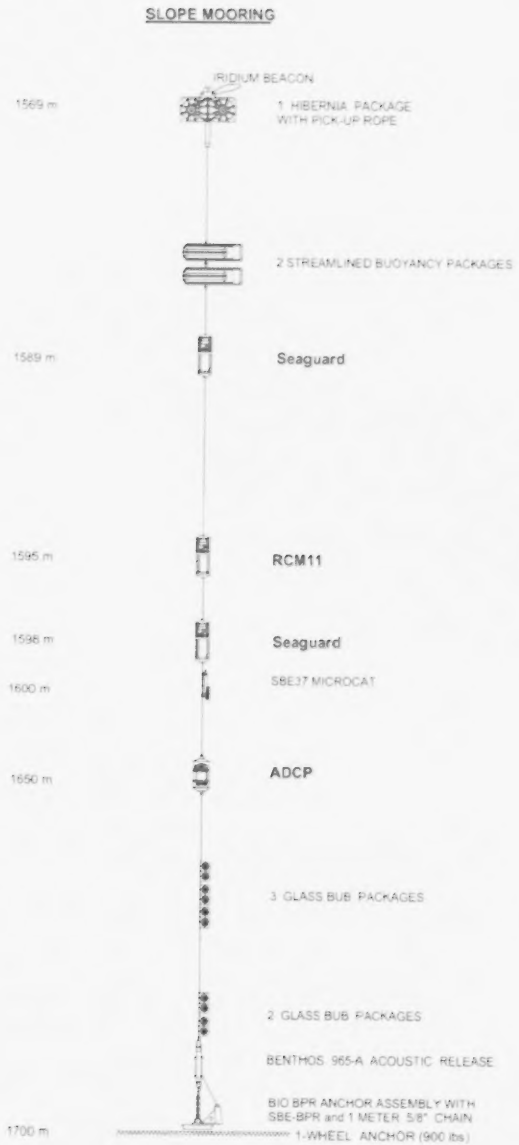

Figure 2: Schematic diagram (not to scale) of mooring 1697.

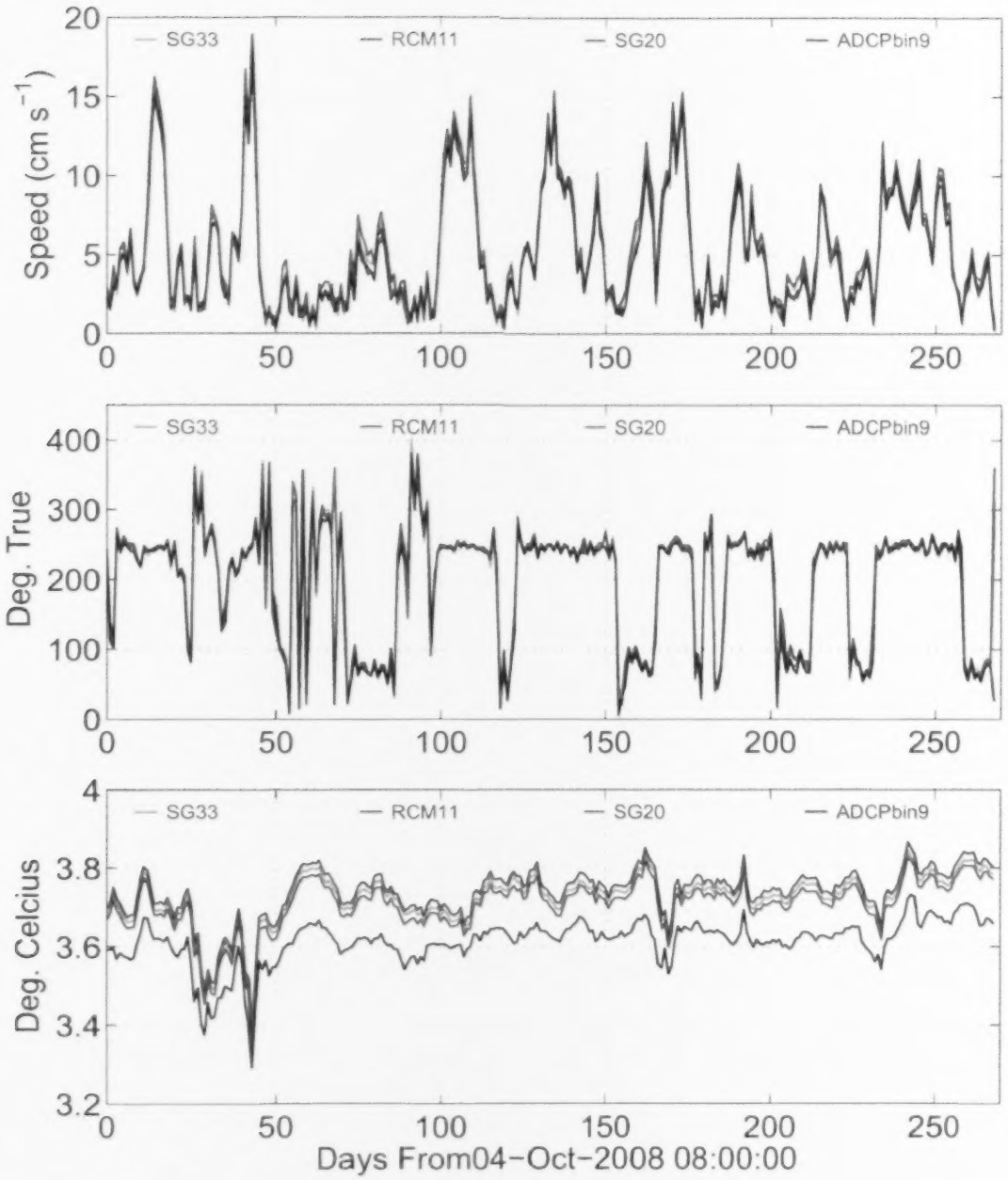

Figure 3: Time series of daily averages of speed (top panel), direction (middle panel) and temperature (bottom panel) reported by the 4 current meters.

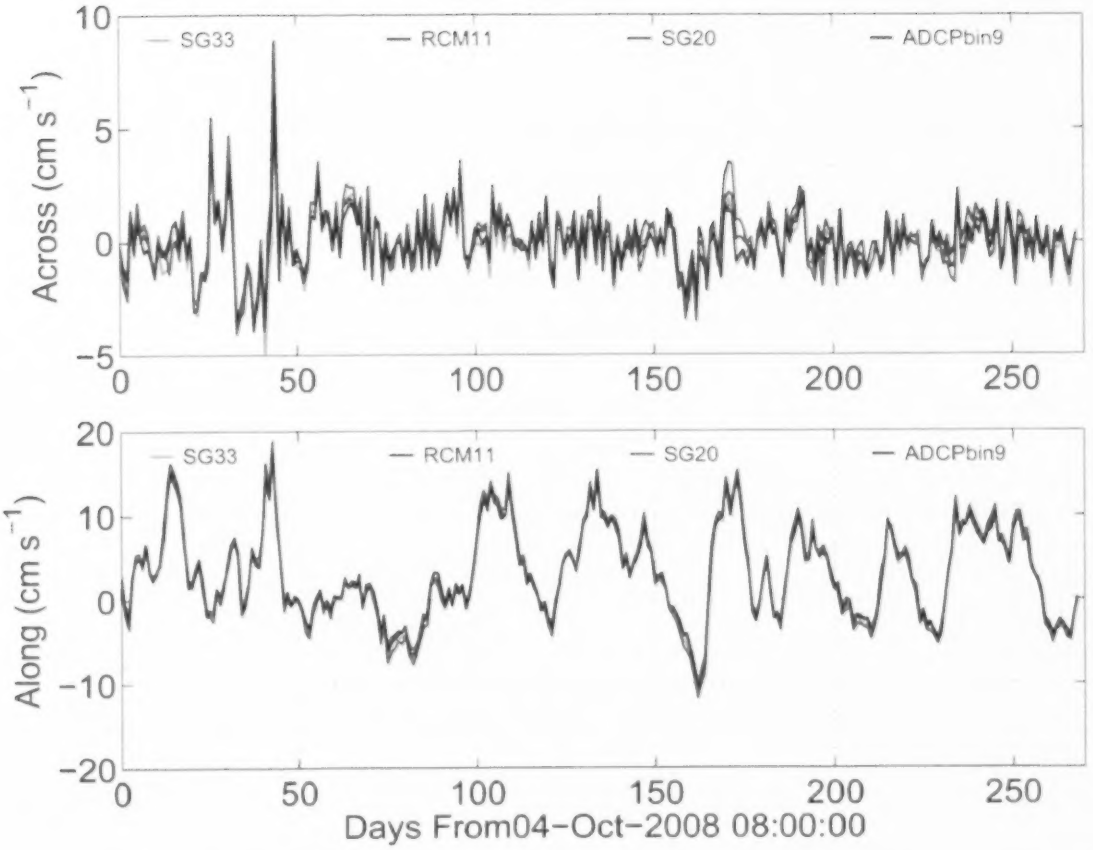

Figure 4: Time series of daily averaged across (top) and along (bottom) shelf components of the current.

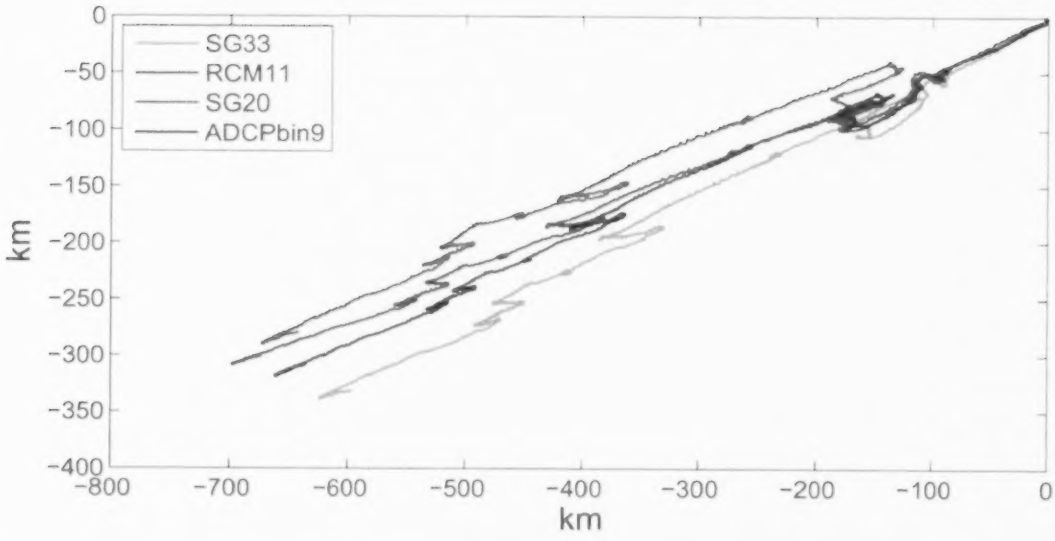

Figure 5: Progressive vector diagram for the four current meters

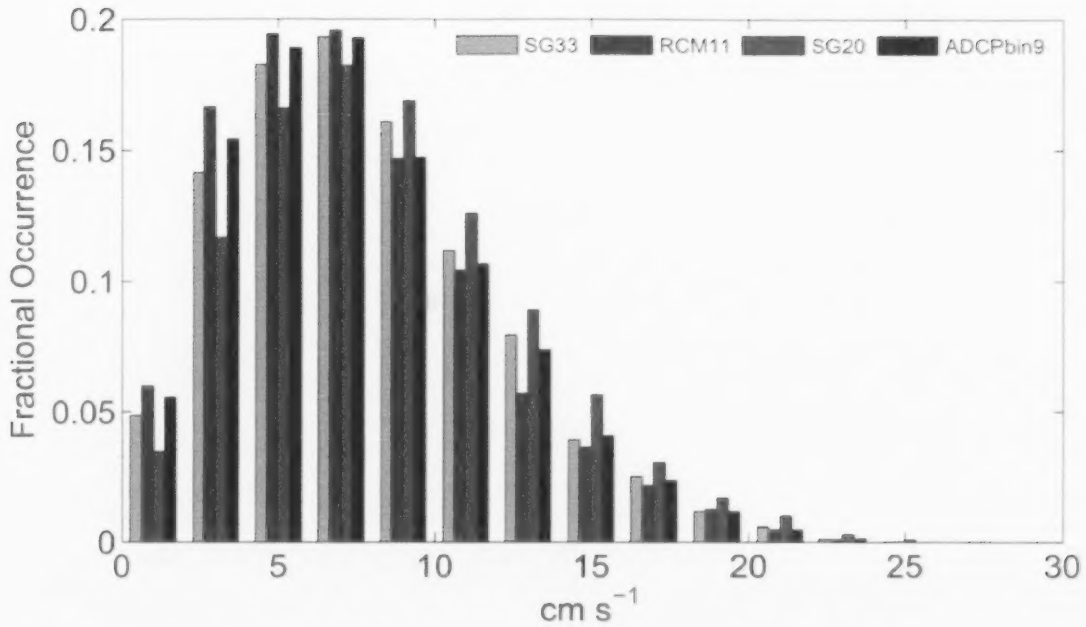

Figure 6: Normalized distribution of current meter speeds binned in 2 cm s^{-1} intervals.

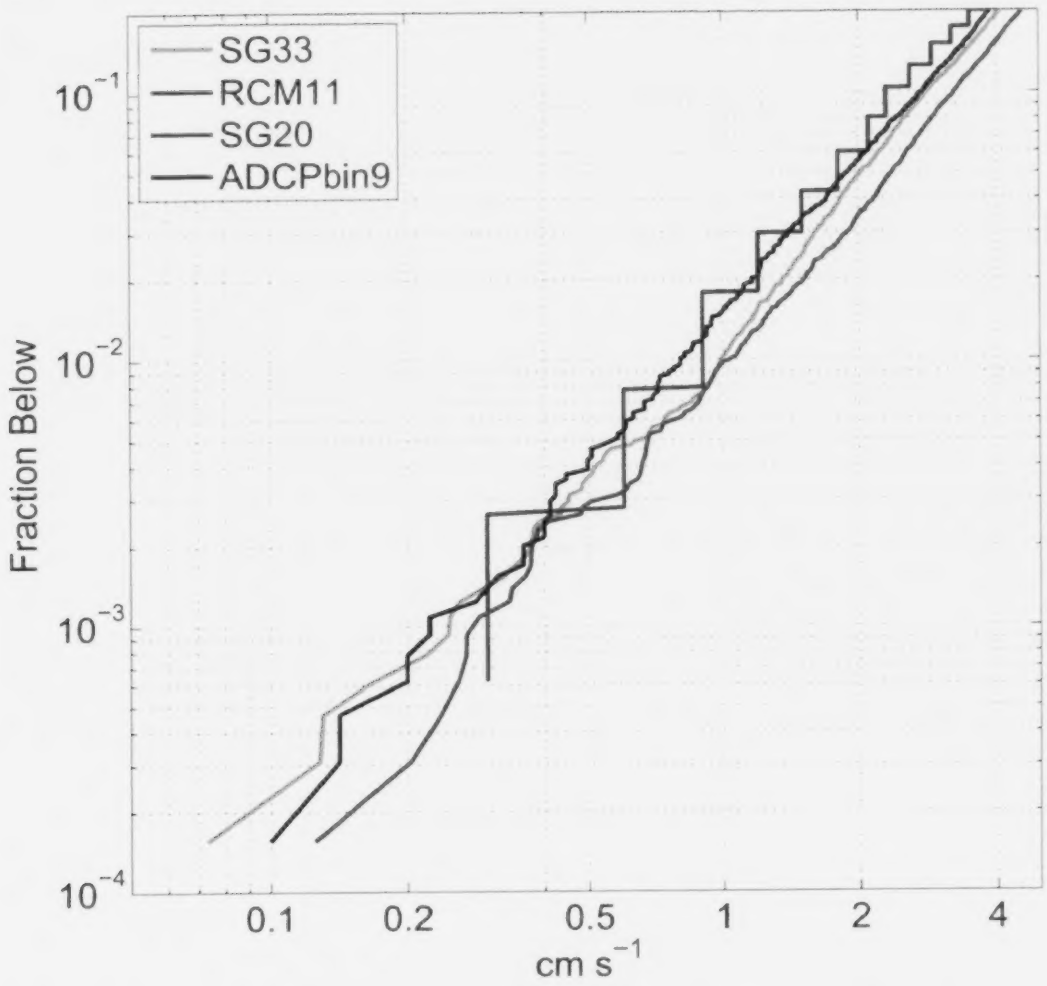

Figure 7: Cumulative speed distribution showing the fraction of observations below particular speeds.

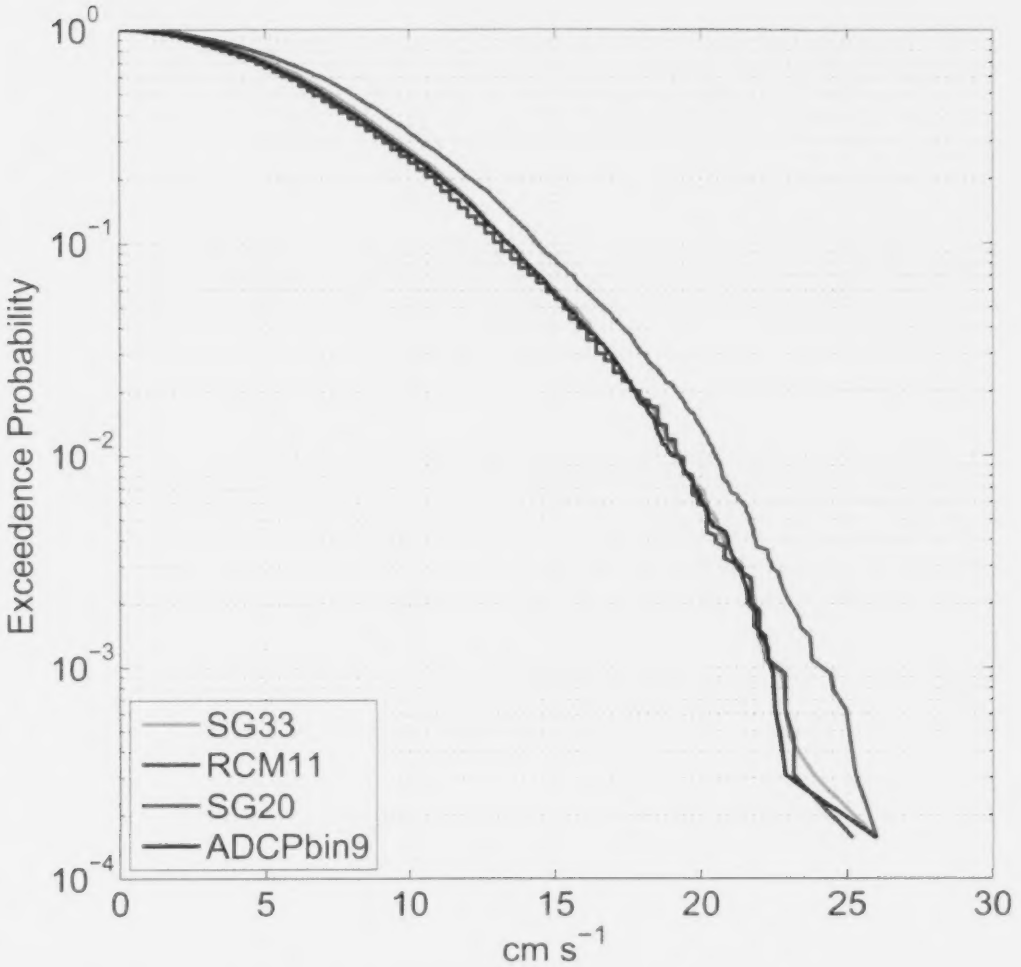

Figure 8: Cumulative speed distribution showing the exceedance probability as a function of speed.

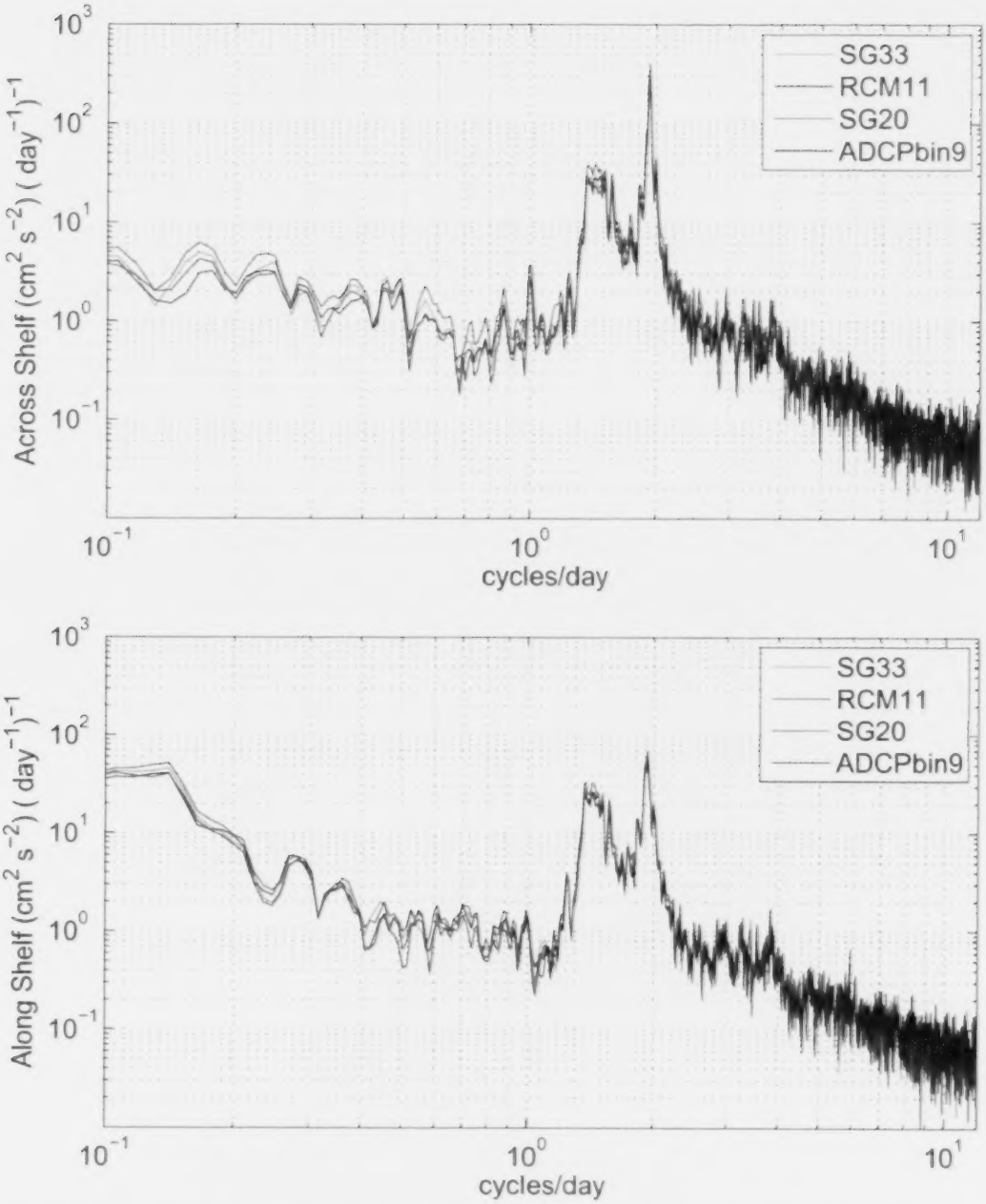

Figure 9: Spectral power distribution expressed as variance per unit frequency for across (top) and along (bottom) shelf current components.

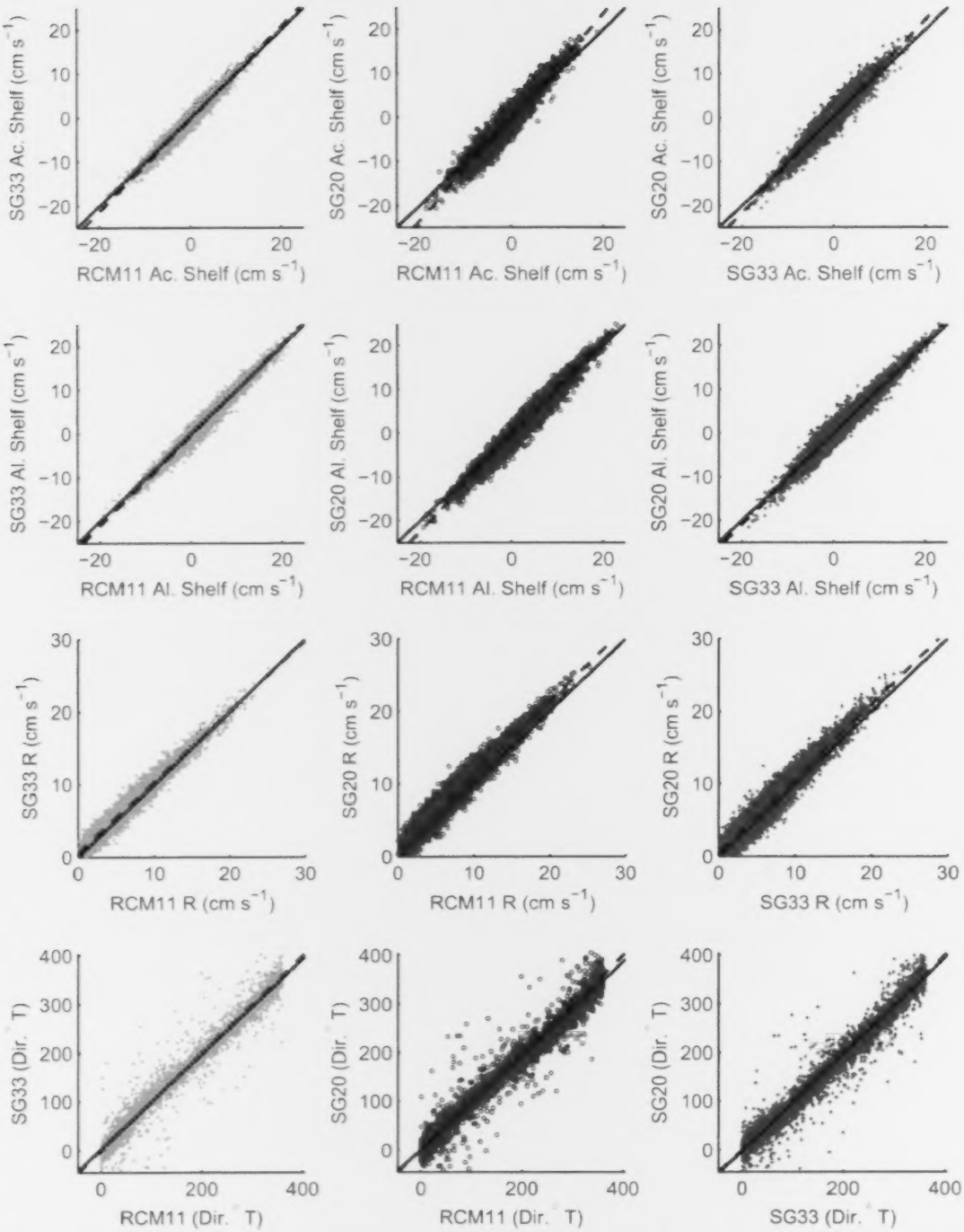
SG33 Ac. Shelf (cm s^{-1})
RCM11 Ac. Shelf (cm s^{-1})
SG20 Ac. Shelf (cm s^{-1})
RCM11 Ac. Shelf (cm s^{-1})
SG20 Ac. Shelf (cm s^{-1})
SG33 Ac. Shelf (cm s^{-1})
SG33 Al. Shelf (cm s^{-1})
RCM11 Al. Shelf (cm s^{-1})
SG20 Al. Shelf (cm s^{-1})
RCM11 Al. Shelf (cm s^{-1})
SG20 Al. Shelf (cm s^{-1})
SG33 Al. Shelf (cm s^{-1})
SG33 R (cm s^{-1})
RCM11 R (cm s^{-1})
SG20 R (cm s^{-1})
RCM11 R (cm s^{-1})
SG20 R (cm s^{-1})
SG33 R (cm s^{-1})
SG33 (Dir. °T)
RCM11 (Dir. °T)
SG20 (Dir. °T)
RCM11 (Dir. °T)
SG20 (Dir. °T)
SG33 (Dir. °T)

Figure 10: Current meter scatter plot for 3 pairings of point measuring instruments. Shown (top to bottom) are the across and along shelf speed components, the speed and the direction. Dashed black line is the regression fit and the solid black line is the equality line.

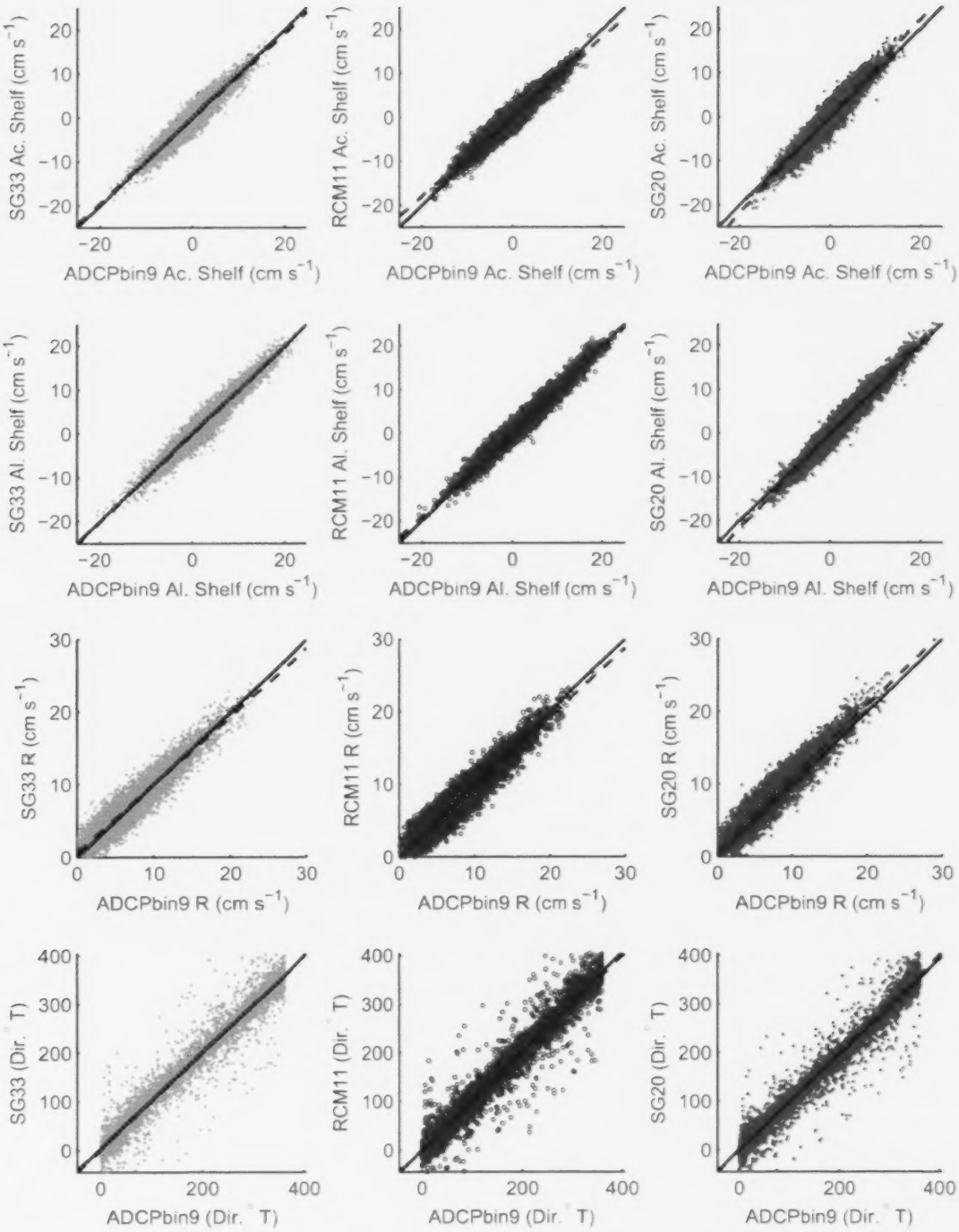
SG33 Ac. Shelf (cm s^{-1})
ADCPbin9 Ac. Shelf (cm s^{-1})
RCM11 Ac. Shelf (cm s^{-1})
ADCPbin9 Ac. Shelf (cm s^{-1})
SG20 Ac. Shelf (cm s^{-1})
ADCPbin9 Ac. Shelf (cm s^{-1})
SG33 Al. Shelf (cm s^{-1})
ADCPbin9 Al. Shelf (cm s^{-1})
RCM11 Al. Shelf (cm s^{-1})
ADCPbin9 Al. Shelf (cm s^{-1})
SG20 Al. Shelf (cm s^{-1})
ADCPbin9 Al. Shelf (cm s^{-1})
SG33 R (cm s^{-1})
ADCPbin9 R (cm s^{-1})
RCM11 R (cm s^{-1})
ADCPbin9 R (cm s^{-1})
SG20 R (cm s^{-1})
ADCPbin9 R (cm s^{-1})
SG33 (Dir. °T)
ADCPbin9 (Dir. °T)
RCM11 (Dir. °T)
ADCPbin9 (Dir. °T)
SG20 (Dir. °T)
ADCPbin9 (Dir. °T)

Figure 11: Current meter scatter plot for 3 pairings of point measuring instruments with bin 9 of the ADCP. Shown (top to bottom) are the across and along shelf speed components, the speed and the direction. Dashed black line is the regression fit and the solid black line is the equality line.

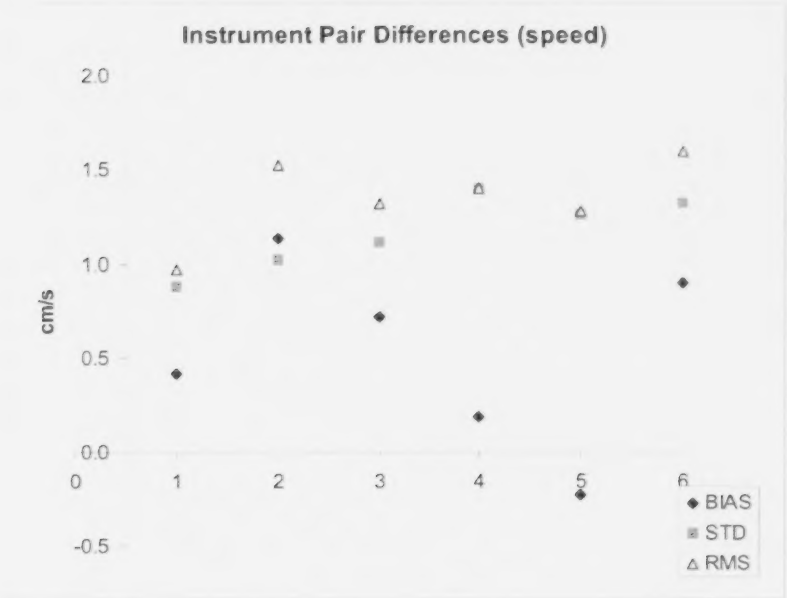

Figure 12: Speed difference statistics for selected pairs: 1=SG33-RCM11, 2= SG20-RCM11, 3=SG20-SG33, 4=SG33-ADCPbin9, 5=RCM11-ADCPbin9 and 6=SG20-ADCPbin9.

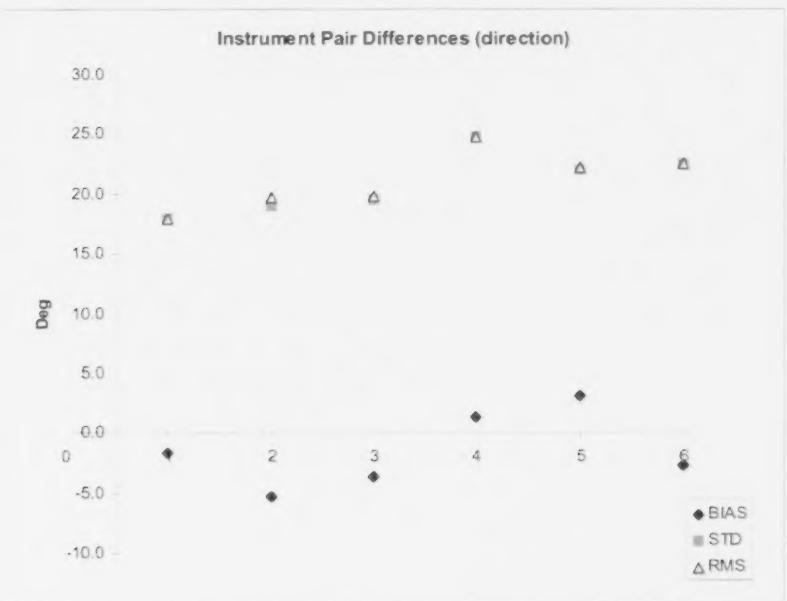

Figure 13: Directional difference statistics for pairs defined in Figure 12.

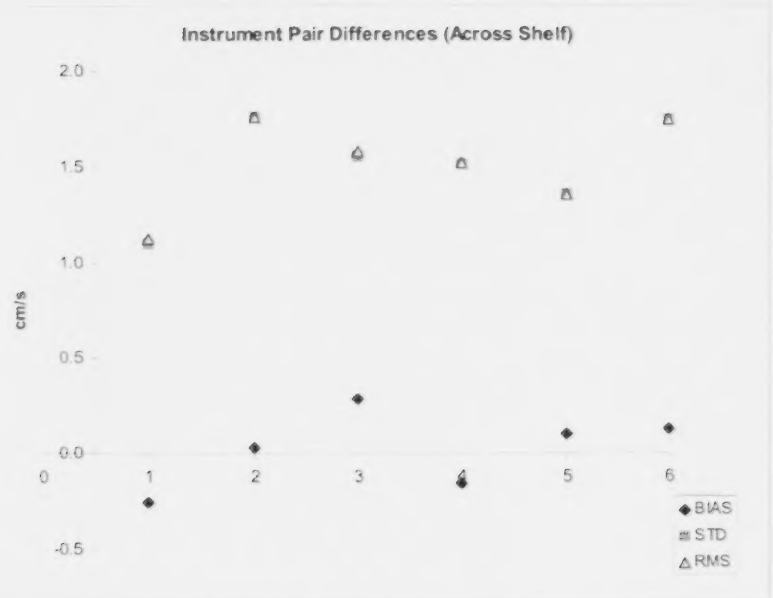

Figure 14: Across shelf current difference statistics for selected pairs defined in Figure 12.

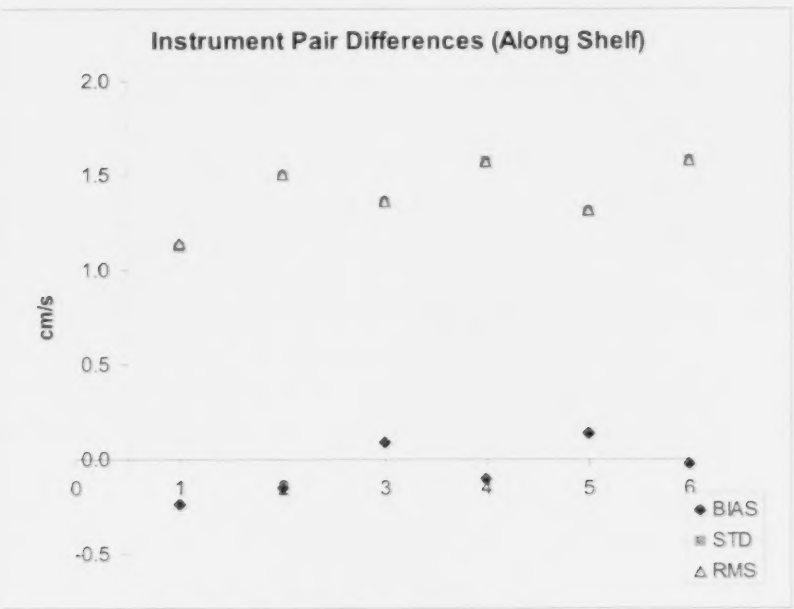

Figure 15: Along shelf current difference statistics for selected pairs defined in Figure 12.

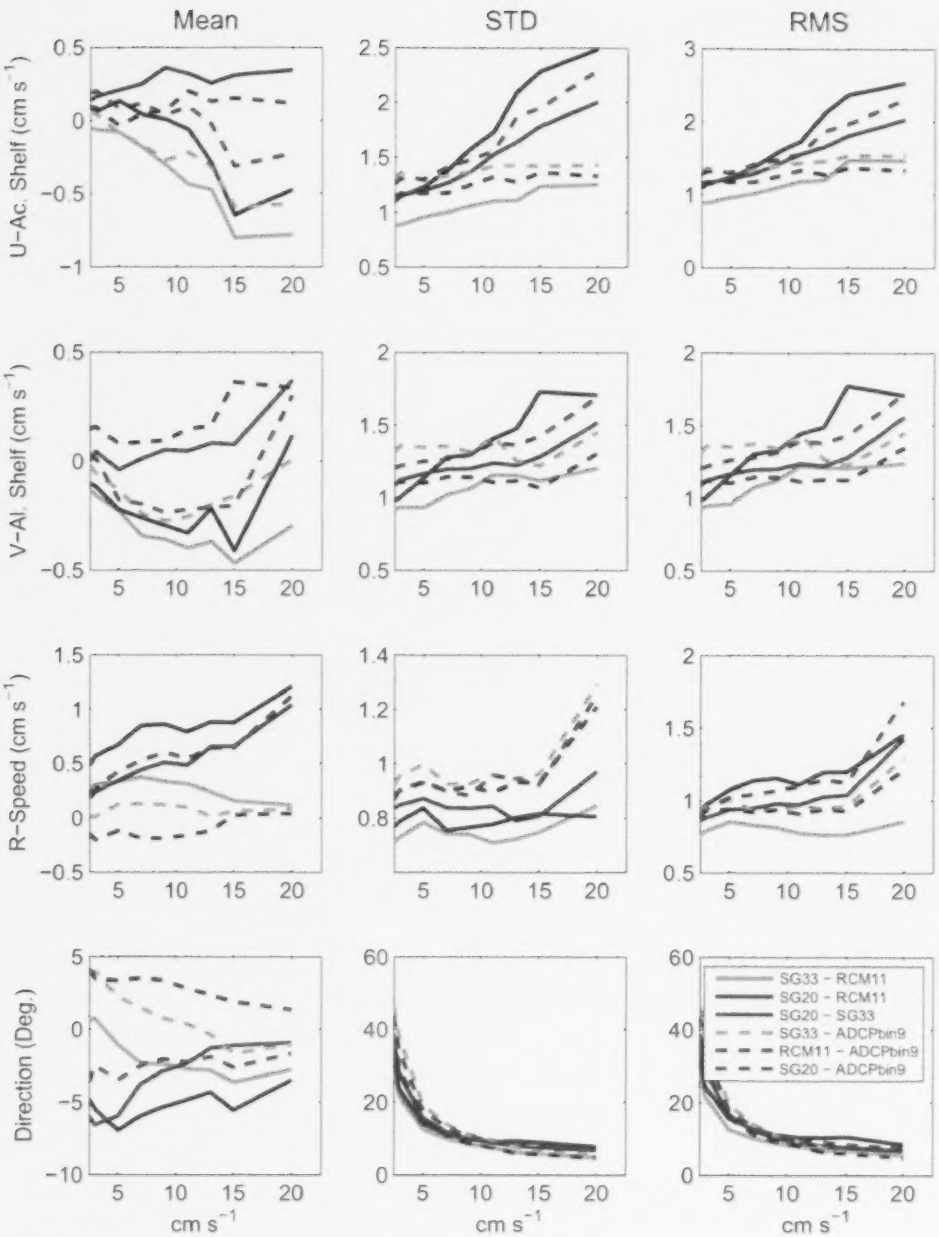

Figure 16: Statistics of instrument pair differences as a function of speed. Shown (top to bottom) are the across and along shelf speed components, the speed and the direction.

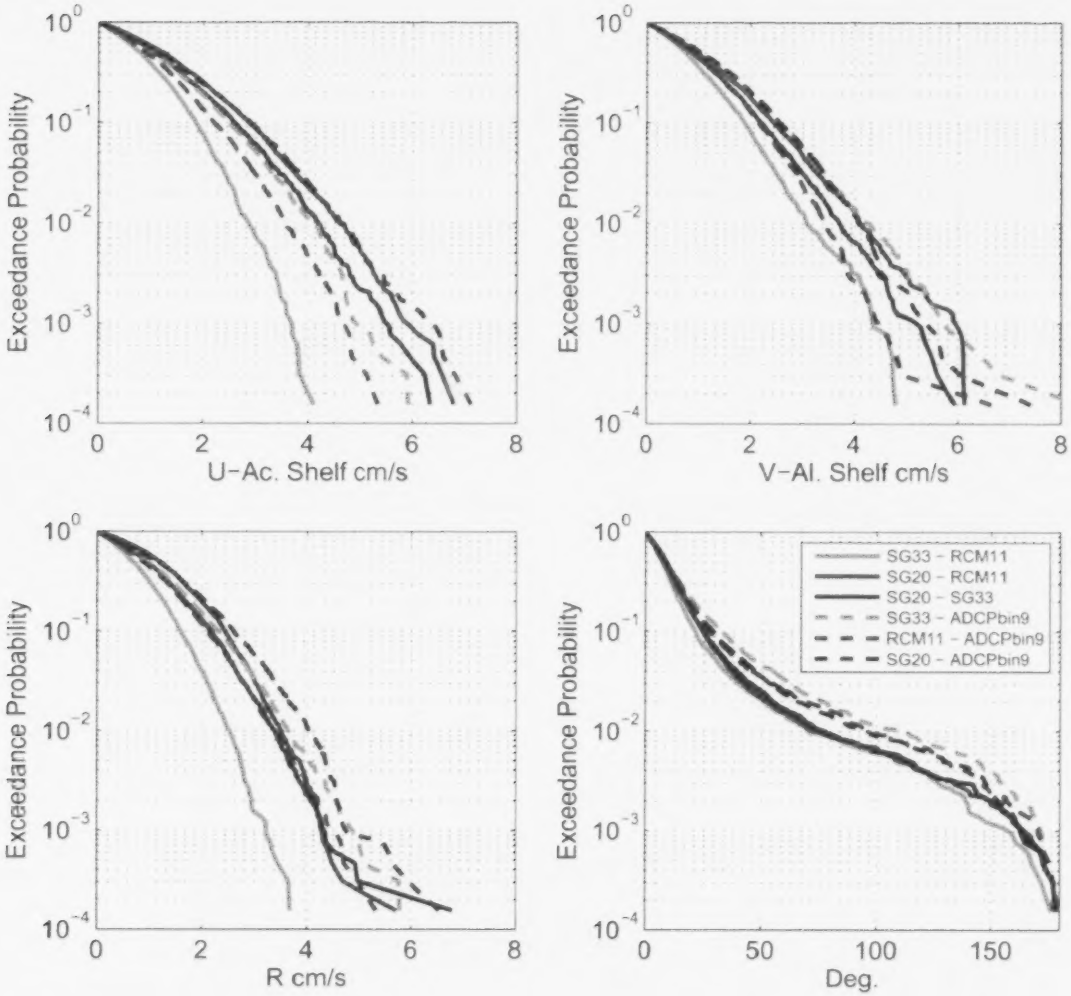

Figure 17: Exceedance probabilities for pair absolute differences.

APPENDIX A: ADCP vertical structure and quality parameters

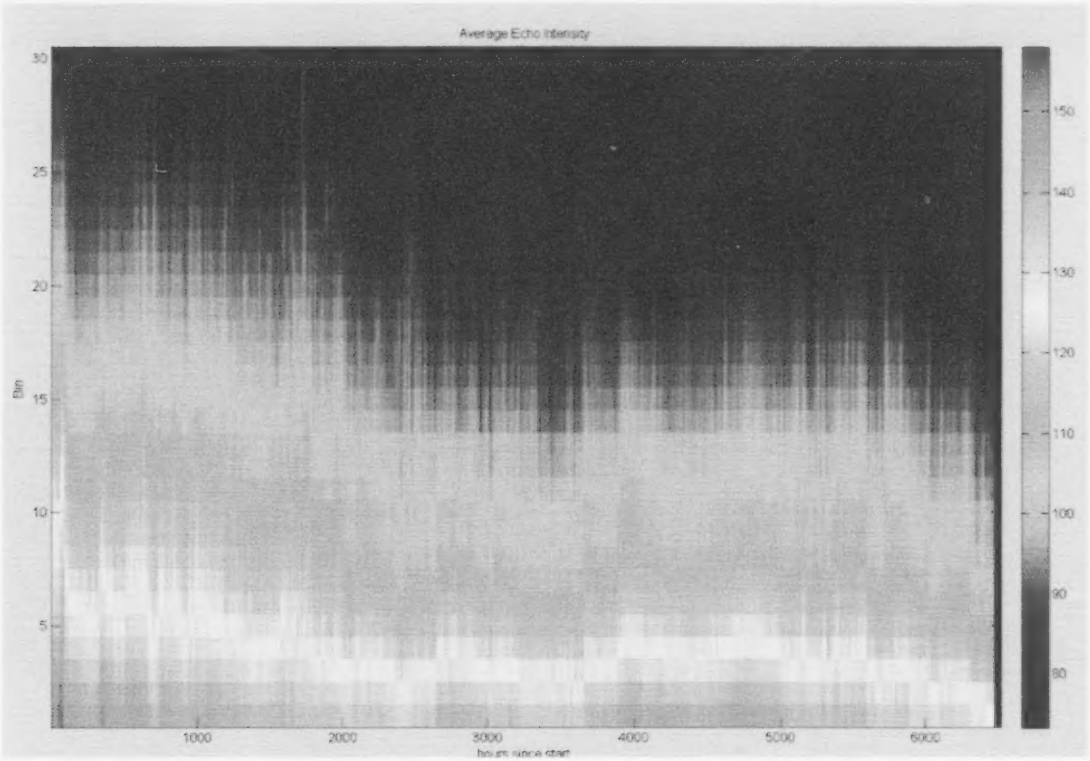

Figure 18: Average echo intensity (counts) recorded by ADCP.

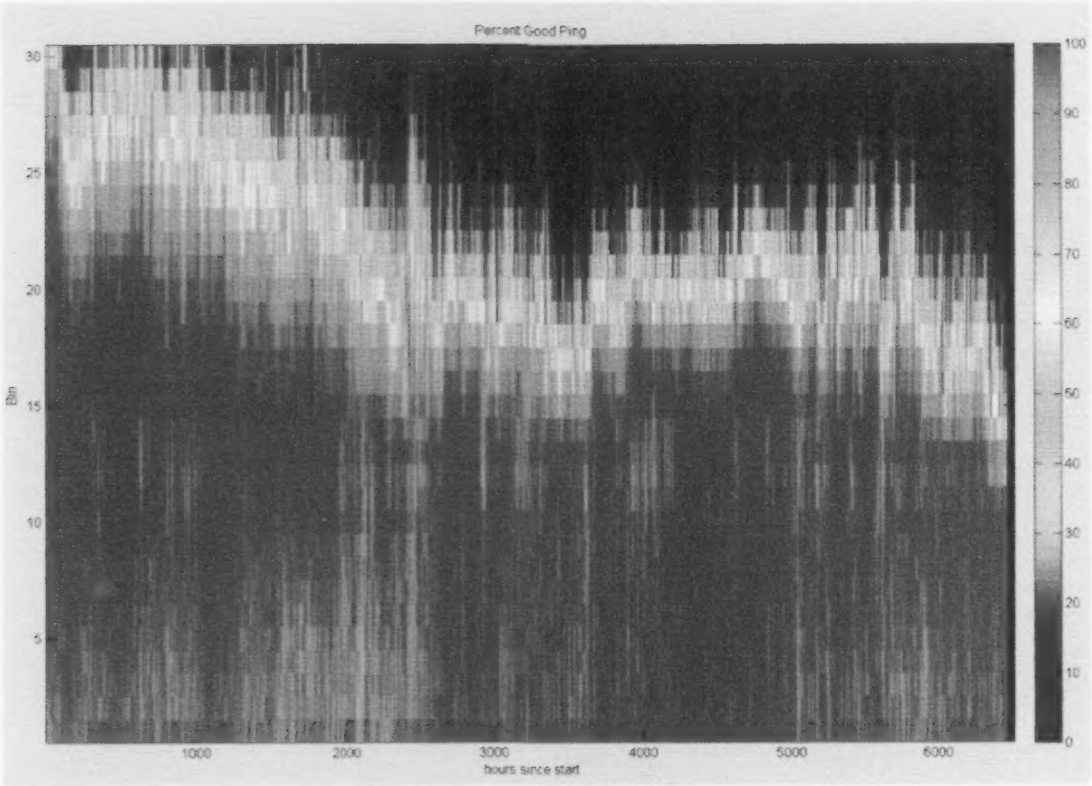

Figure 19: Percent good pings recorded by ADCP.

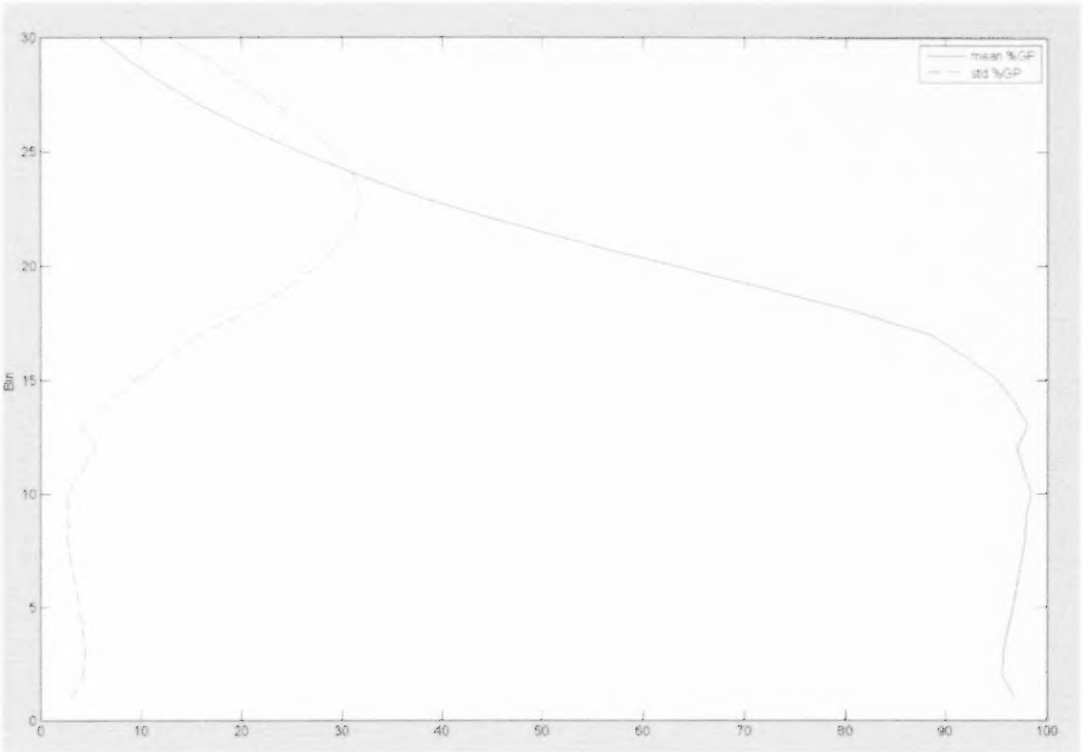

Figure 20: Mean and standard deviation of percent good pings for each bin

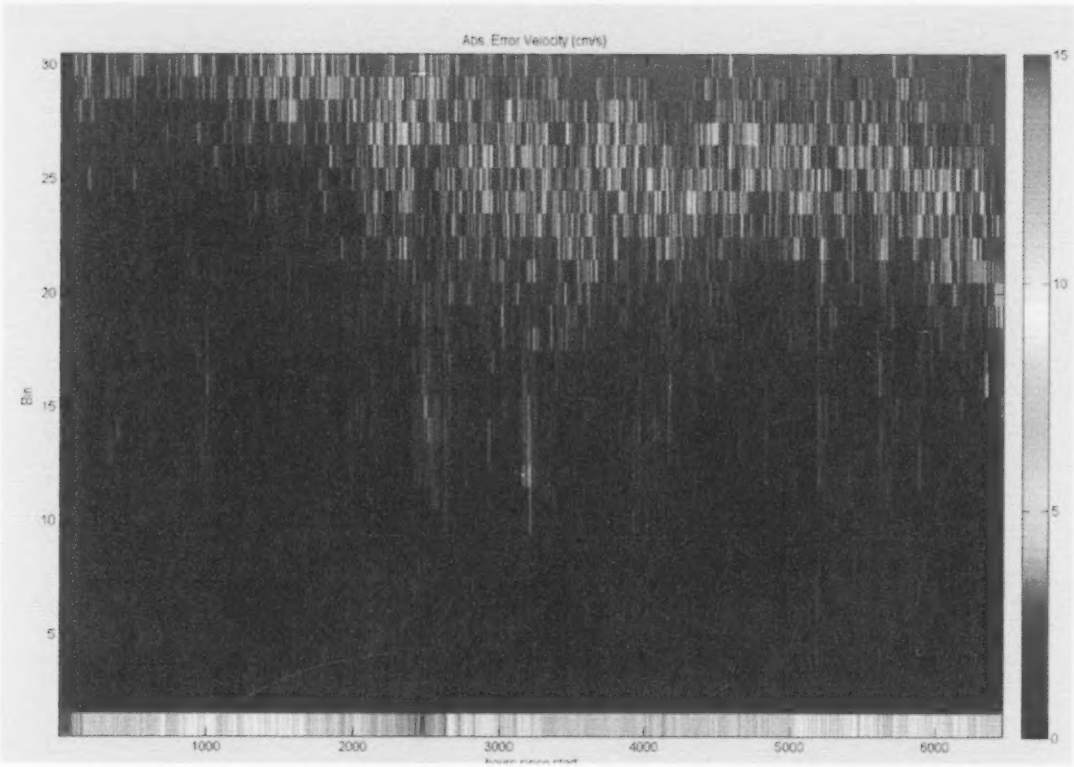

Figure 21: Absolute error velocity (cm s^{-1}) recorded by the ADCP.

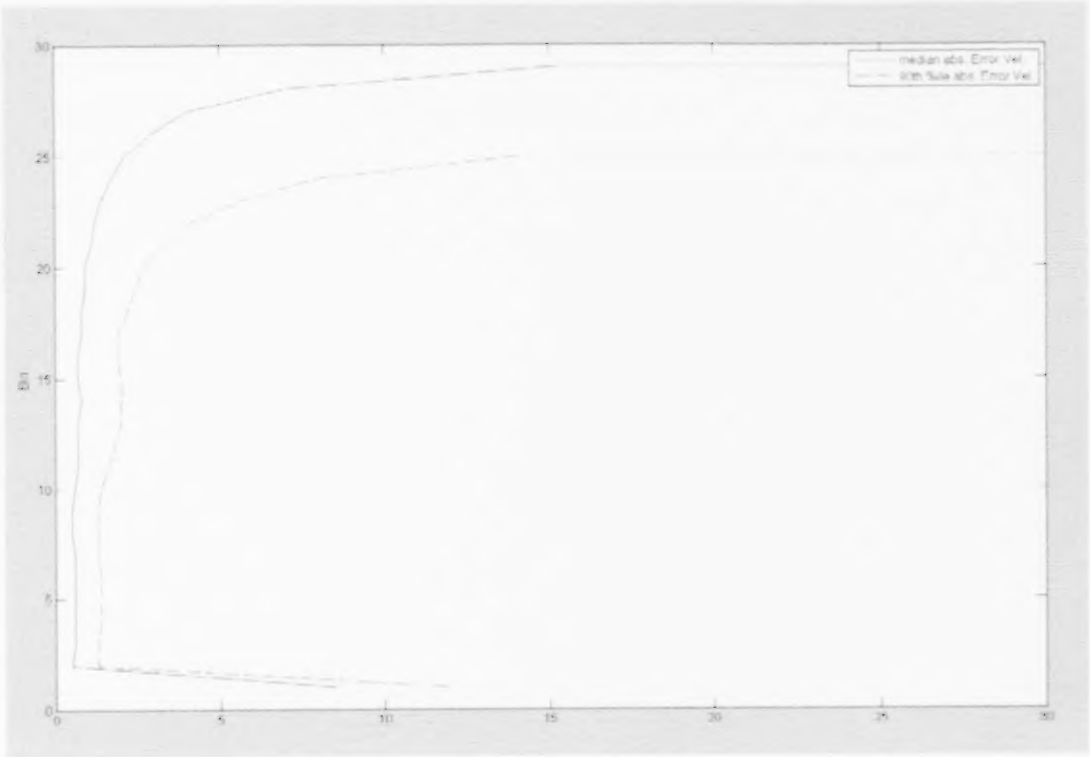

Figure 22: Median and 90th percentile of absolute error velocity (cm s^{-1}) for each bin.

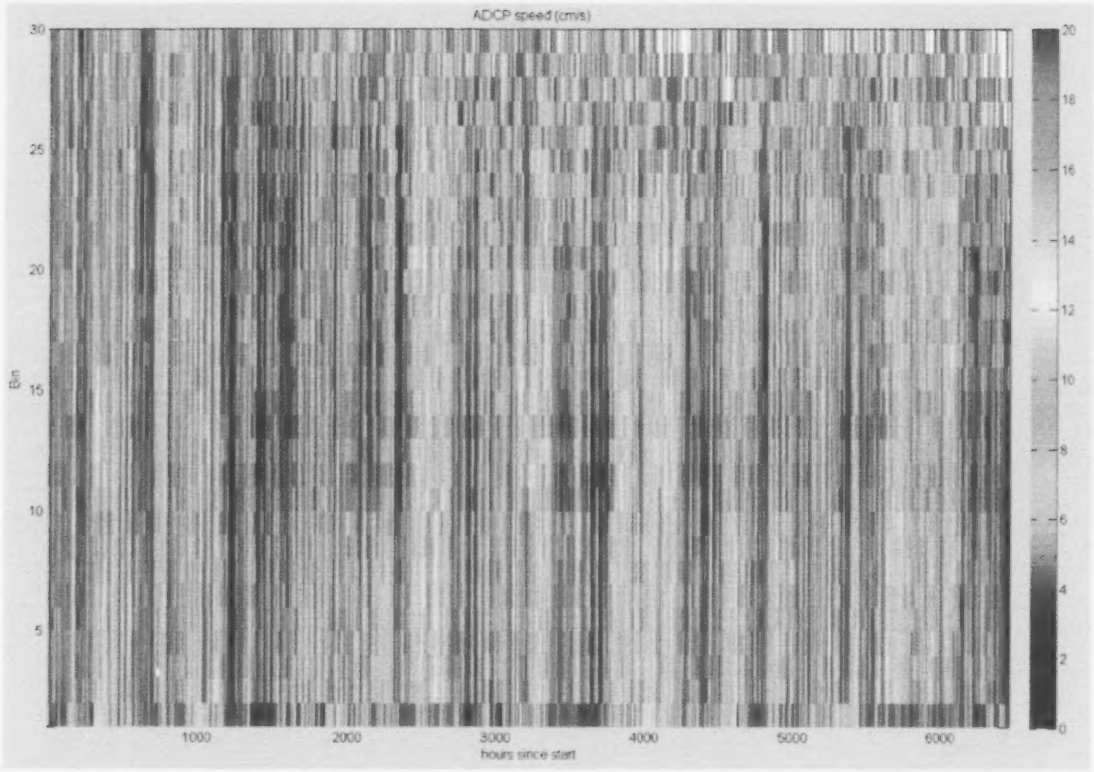

Figure 23: Vertical time structure of ADCP speed.

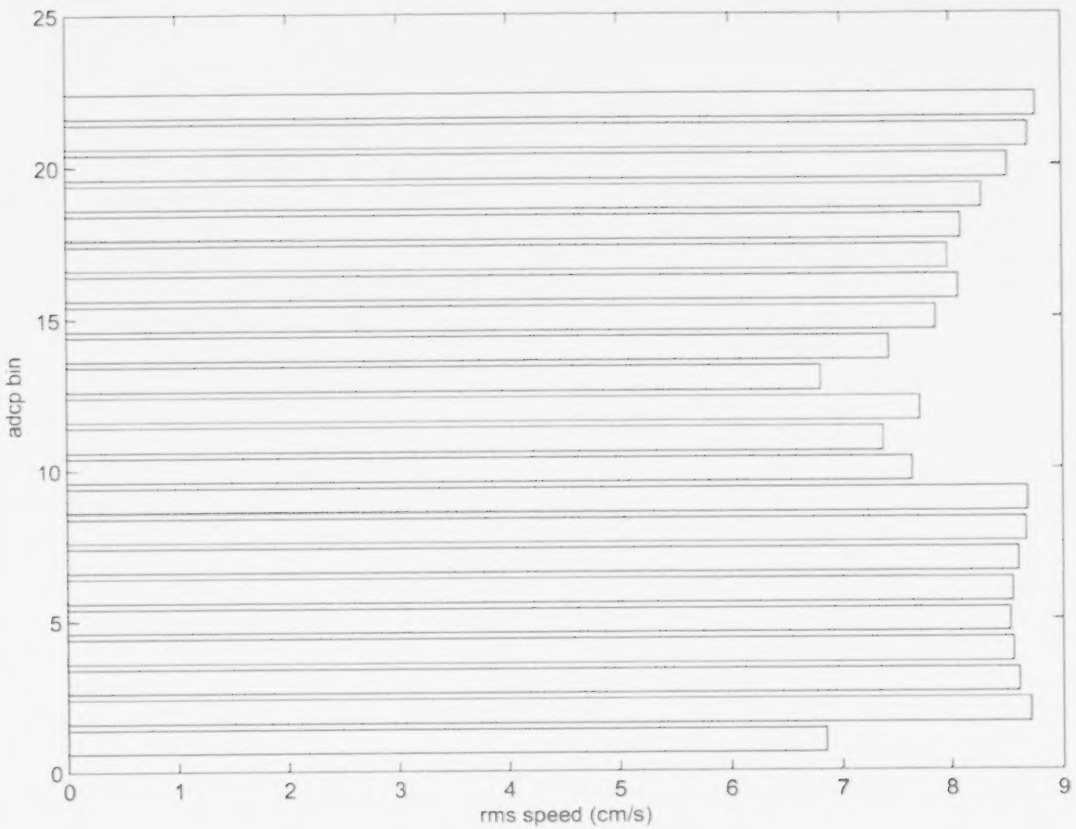

Figure 24: Vertical structure of the ADCP RMS speed.

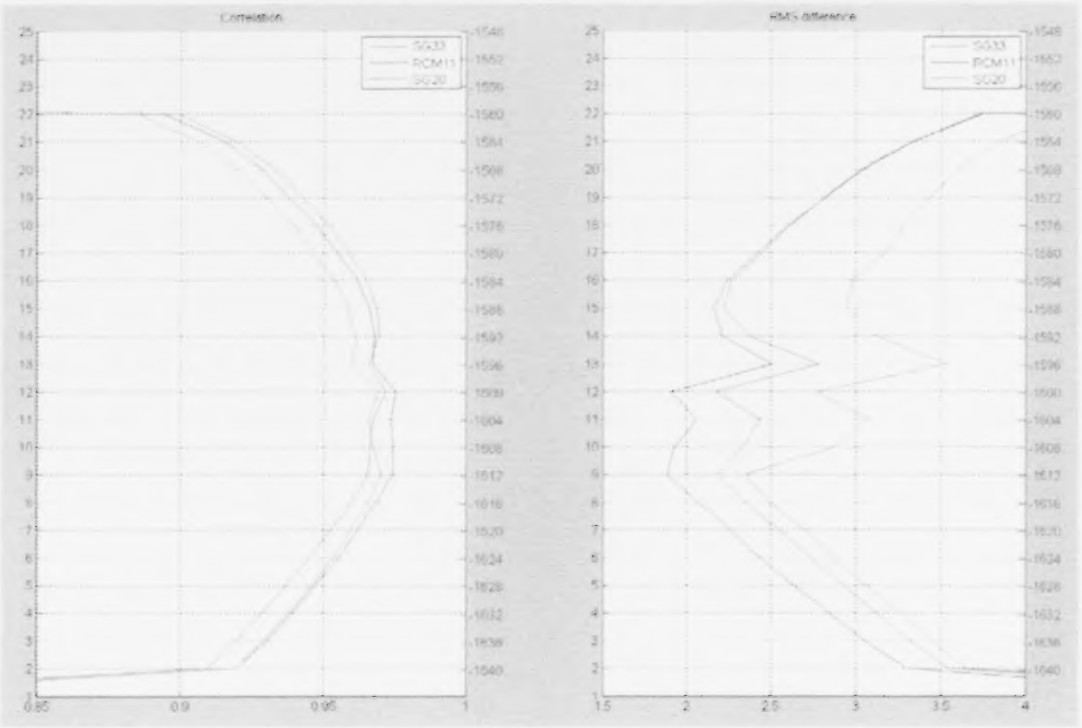

Figure 25: Vertical structure of the correlation and RMS difference of each point instrument with ADCP bins. Vertical units are bin number on left and depth in meters on the right.

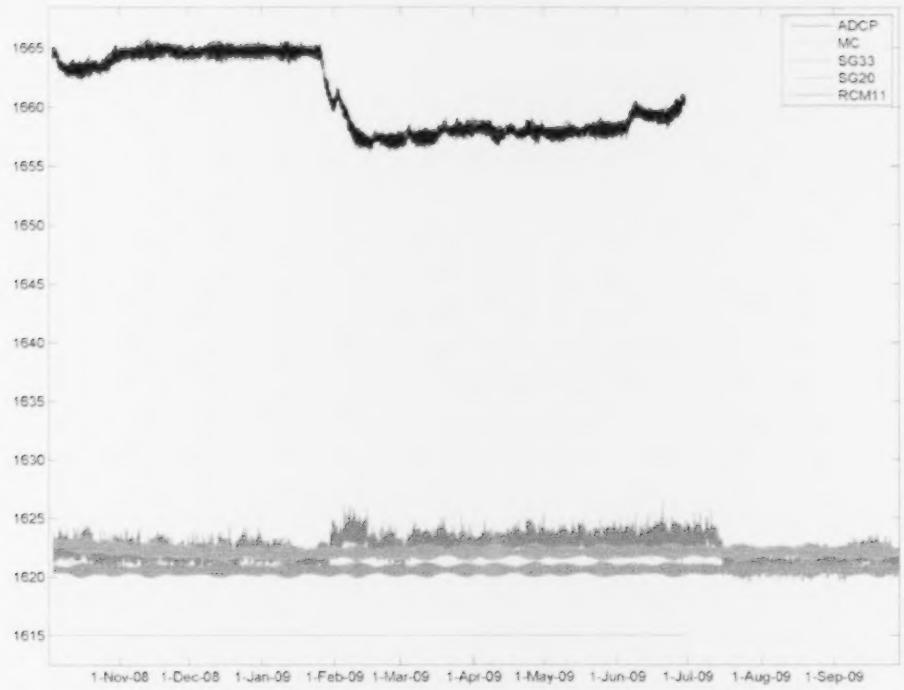

Figure 26: Pressure time series from instruments (NB: for illustrative purpose only; some records were not corrected for air pressure, for actual depths refer to mooring diagram).

APPENDIX B: Temperature Comparison

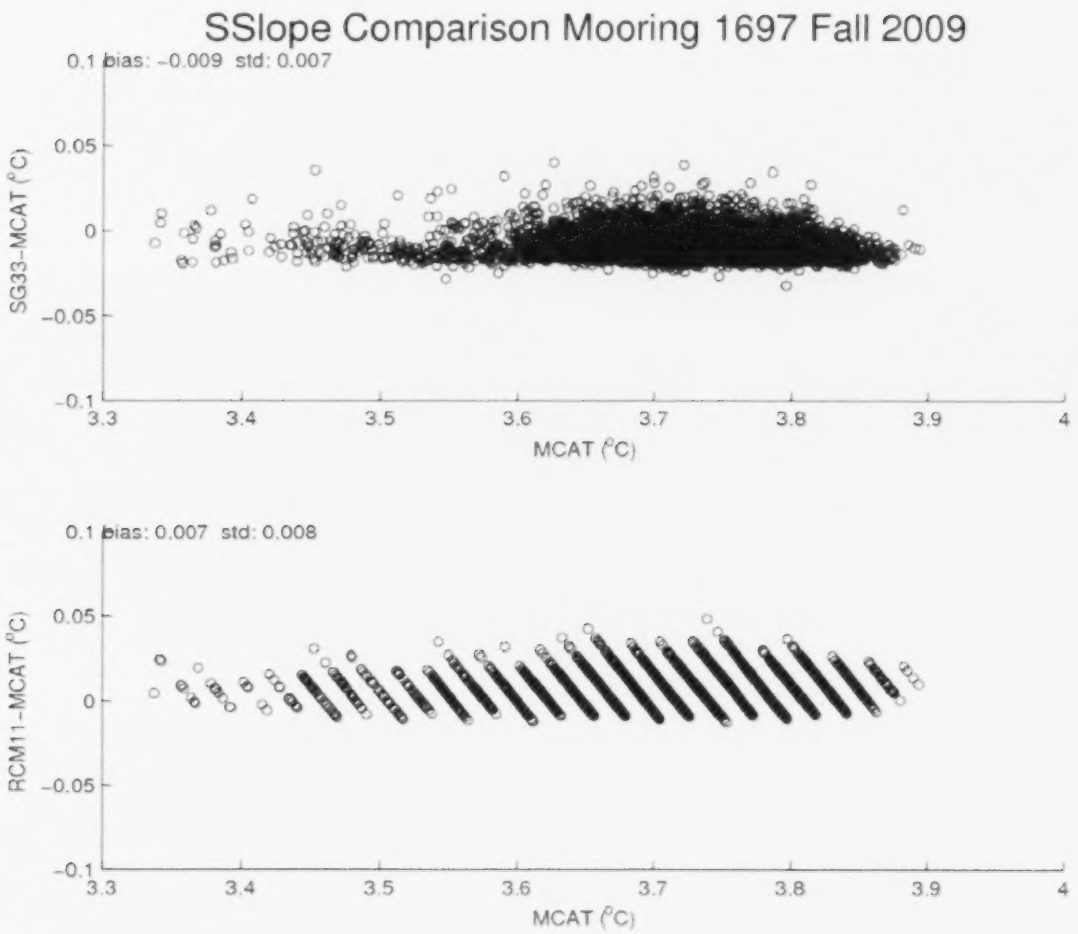

Figure 27: Differences between current meter temperatures (upper Seaguard and RCM11) and MicroCAT temperature. Scotian slope deployment.

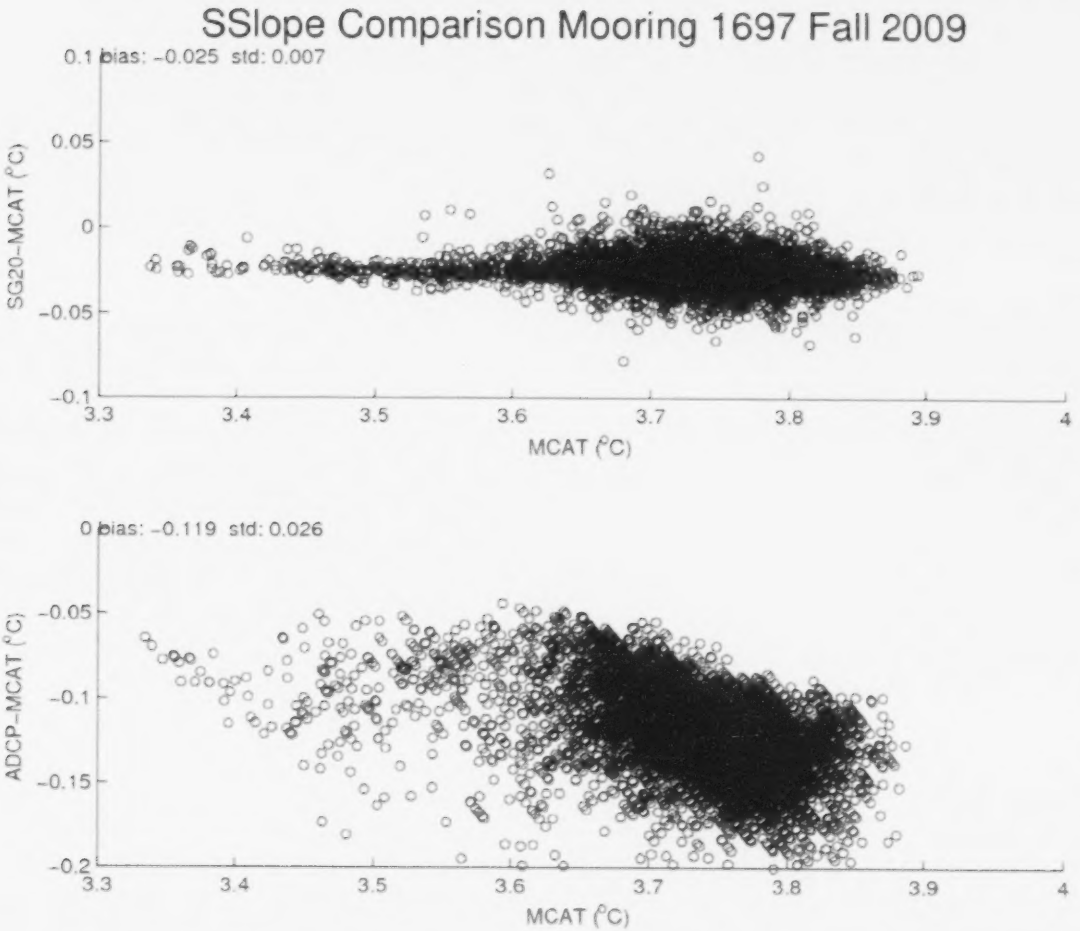

Figure 28: Differences between current meter temperatures (lower Seaguard and ADCP) and MicroCAT temperature. Scotian slope deployment.

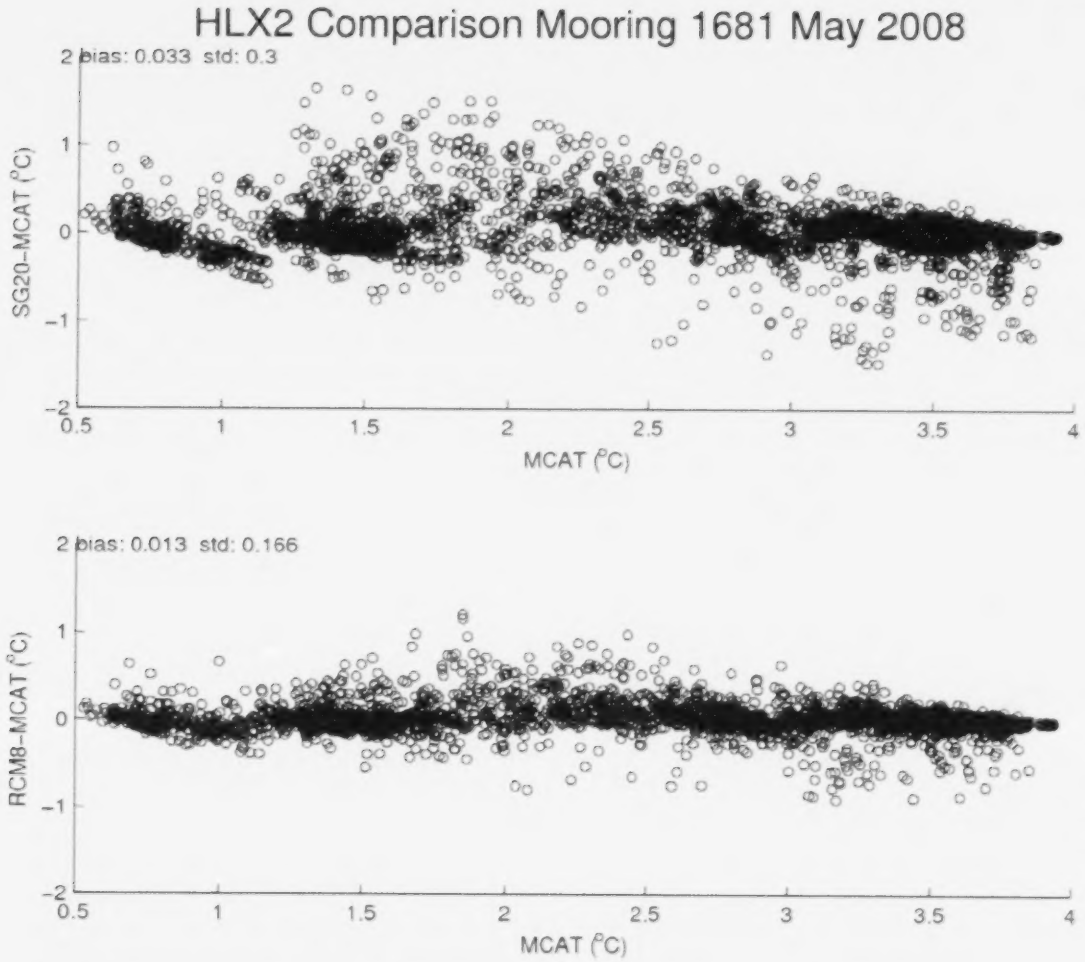

Figure 29: Differences between current meter (lower Seaguard and RCM8) and MicroCAT temperature. Scotian Shelf deployment.

APPENDIX C: Distribution of Instrument Differences

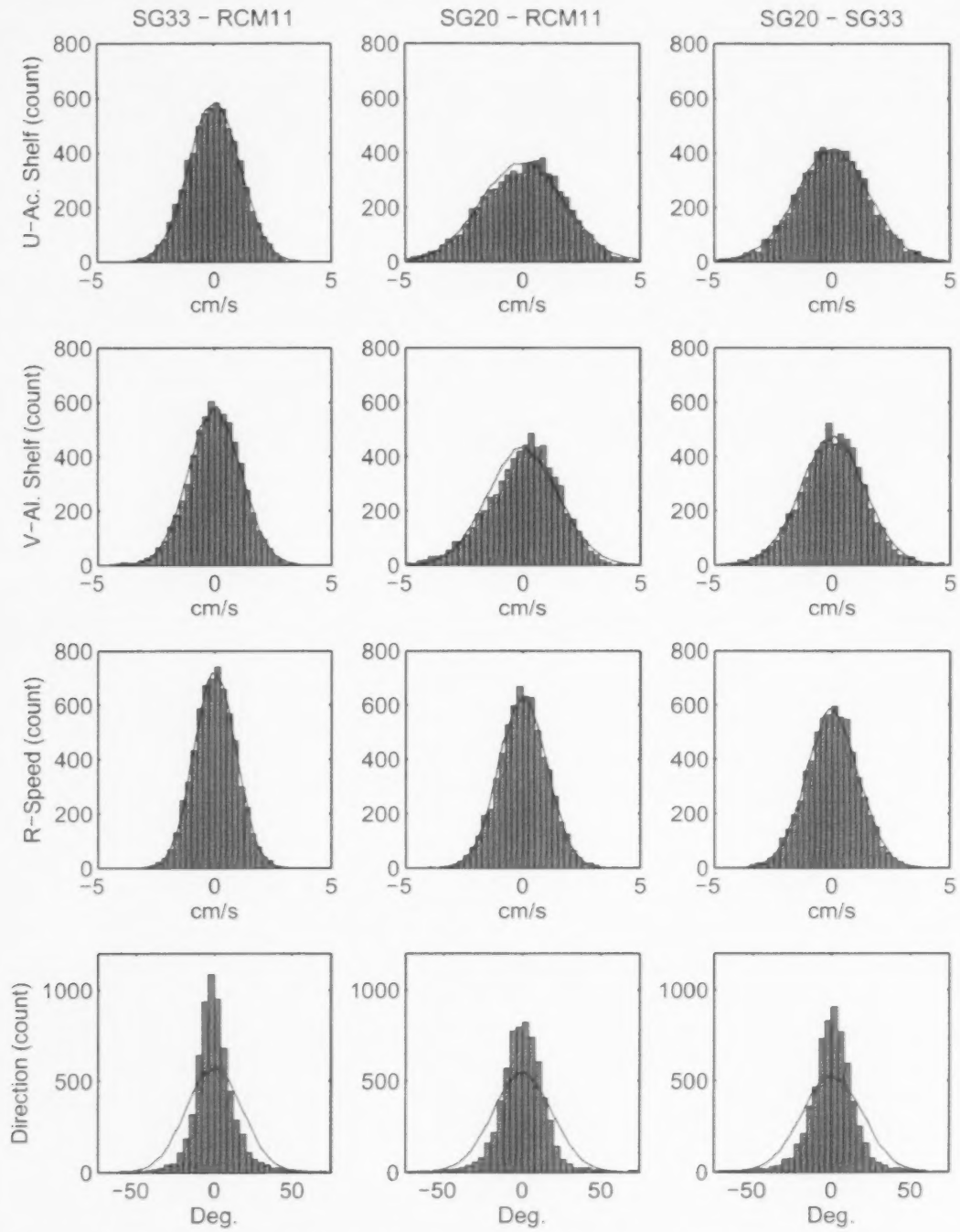

Figure 30: Distributions of point instrument differences. Solid line is the normal (Gaussian) distribution fit (computed from the mean and STD of the data).

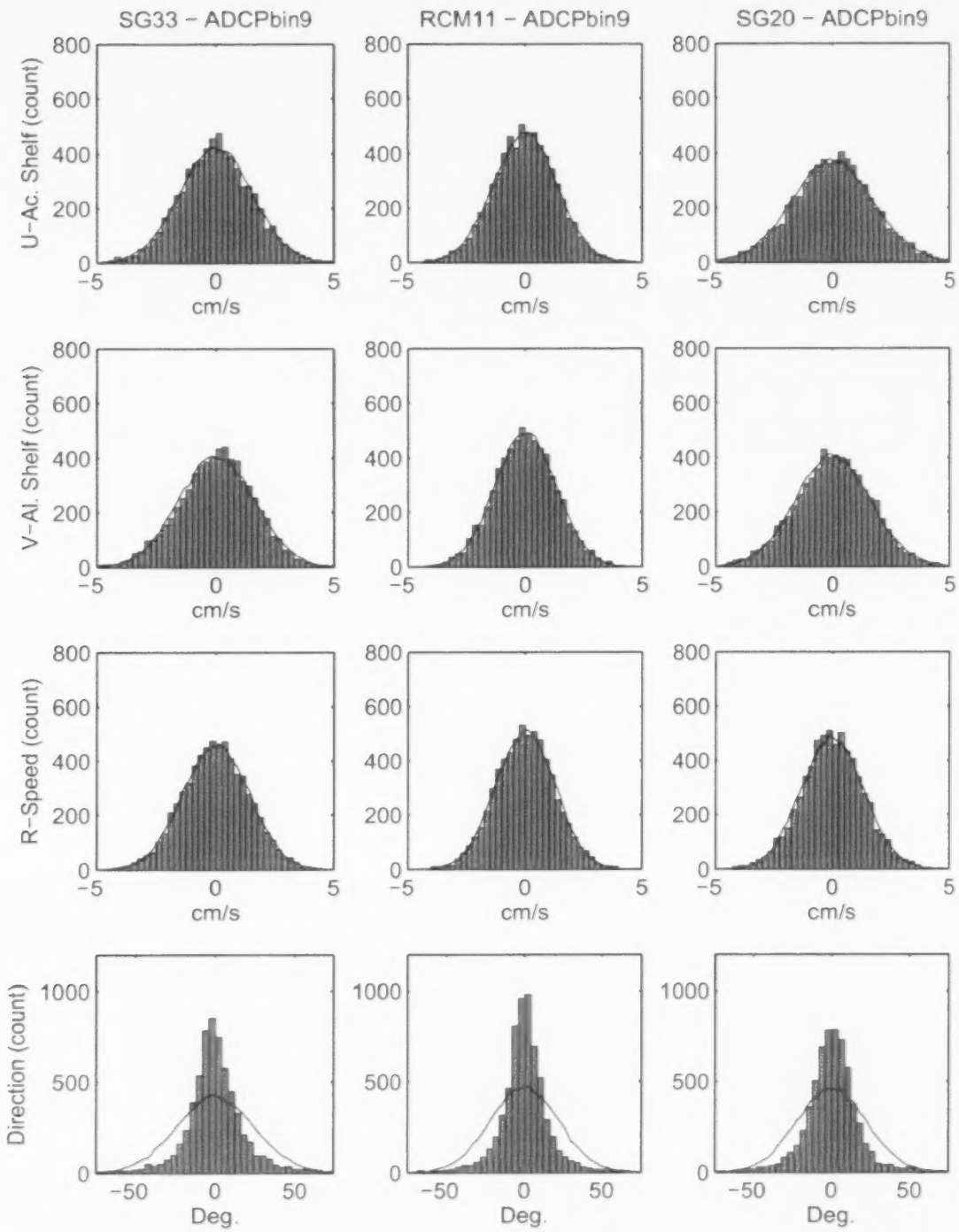

Figure 31: Distributions of ADCP and point instrument differences. Solid line is the normal (Gaussian) distribution fit (computed from the mean and STD of the data).

APPENDIX D: Low Speed Amplification of Directional Error

In an acoustic instrument, the direction of flow is determined by the relative magnitude of the current components (U,V in instrument frame) and actual compass reading, ϕ_c. From basic calculus and statistics, the mean square error can be shown to be:

$$d\phi^2 = (\frac{\partial\phi}{\partial U})^2 dU^2 + (\frac{\partial\phi}{\partial V})^2 dV^2 + (\frac{\partial\phi}{\partial\phi_c})^2 d\phi_c^2$$

The task now is to fill in the the partial derivatives. The angle can be expressed as

$$\phi = tan^{-1}(U/V) + \phi_c$$

From which the partial derivatives are determined to be:

$$\frac{\partial\phi}{\partial U} = \frac{V}{U^2+V^2}$$

$$\frac{\partial\phi}{\partial V} = -\frac{U}{U^2+V^2}$$

$$\frac{\partial\phi}{\partial\phi_c} = 1$$

The speed is

$$S^2 = U^2 + V^2$$

hence

$$d\phi^2 = \frac{V^2}{S^4} dU^2 + \frac{U^2}{S^4} dV^2 + d\phi_c^2$$

It can be shown in a similar derivation that

$$dS^2 = \frac{U^2}{S^2}dU^2 + \frac{V^2}{S^2}dV^2$$

We can assume the horizontal errors dU and dV are equal which leads to the final result

$$d\phi^2 = \frac{dS^2}{S^2} + d\phi_c^2$$